Gel-mobility assays of cysteine mutants in the C-terminus region of the *Neurospora crassa* large subunit of ribonucleotide reductase

By

Mojgan Siahbazi

A dissertation
submitted to the Faculty of Graduate Studies and Research
in partial fulfillment of the requirements for the degree of
Master of Science in Biology

Carleton University

Ottawa, Ontario

Your file Votre référence
ISBN: 978-0-494-44140-4
Our file Notre référence
ISBN: 978-0-494-44140-4

ABSTRACT

Ribonucleotide reductase (RNR) catalyzes the conversion of ribonucleotides to deoxyribonucleotides (NDPs to dNDPs) and thus plays an essential role in DNA synthesis, replication and repair. The large subunit of RNR in *Neurospora crassa* is unusual in that it is also involved in nonself recognition. In this fungus, two allelic forms of this gene occur, designated as *un-24*^{PA} and *un-24*^{OR}. Co-expression of these allelic forms in the same cell results in the formation of non-reducible UN-24 protein complexes and cell death. It was previously determined that three conserved cysteines in the C-terminus region of UN-24 are important for protein complex formation. In order to characterize this domain, a region coding for 102 amino acids of the C-terminus portion of un-*24*^{PA} was cloned and expressed in the pQE31 *E. coli* expression vector. The expressed protein resolved as multiple bands in SDS-PAGE, each larger than the predicted size. Seven mutants of cysteine residues involved in both catalytic and nonself recognition functions of UN-24 were created and protein size and electrophoretic patterns of these expressed proteins were examined under non-reducing and reducing conditions. These simple mutational changes altered the electrophoretic patterns of the expressed proteins suggesting that post-translational modifications involve these cysteines.

ACKNOWLEDGMENTS

I would like to thank my supervisor, Dr. Myron Smith, for his support throughout my masters program. Working on this research with Myron was fun, interesting, and full of lessons to learn. Thank you Myron for teaching me how to work diligently and patiently, for making me interested in my research, for advising me hours and hours toward my work without getting tired.

I would like to thank my committee adviser, Dr. Bill Willmore, for his professional advices and comments regarding the subject of my thesis. Special thanks to Dr. John Vierula for generously providing materials and encouragements.

I also would like express my appreciation to Dr. Sharon Regan, Dr. Buchanan and Susan Elizabeth Buchanan for motivations and advices.

I am grateful to extend a sincere thanks to my friends and lab mates; Kenji Wellman, Zahra Arzhangi and Dave Chitty for technical assistance; Hannah Mirrashed for her insight, support, and great friendship; Rob Smith, Dennis Lafontaine, and Fuad Tanha, for being patient in answering to my questions. A warm thanks to Lucie Labelle, for her great friendship and help over the last year. I wish all the best for you all.

I leave a special note to my family. To my father and mother, for their love, support, and encouragement during doing this work and my personal tribulations. To my brothers for being kind and supportive all these years.

Finally to my little girl, my heart and my beautiful Kimia, for leaving me with the strength and comfort to do this work more pleasant and joyfully, I love you more than anything in the world.

TABLE OF CONTENTS

Abstract ii
Acknowledgements iii
Table of Contents iv
List of Figures v
List of Tables vi

1. Introduction 1
1.1 Heterokaryon incompatibility loci 2
1.2 Characteristics of self-incompatible transformants 5
1.3 Escape from heterokaryon incompatibility and mechanism 12
1.4 Ribonucleotide reductase (RNR) 18
1.5 Proposed incompatibility mechanism of *un-24* 20

2. Thesis Objective 26

3. Materials and Methods 26
2.1 *un-24* constructs, microbial strains, and growth conditions 26
2.2 Primers and PCR amplifications 27
2.3 Rolling circle Site-directed mutagenesis 29
2.4 Protein expression assays 32
2.5 SDS polyacrylamide gel electrophoresis (SDS-PAGE) 33
2.6 Coomassie staining 34
2.7 Western blot analysis and immunoblot detection 34
2.8 Protein minipreps of 6x His-tagged proteins under native condition 35

4. Results 37
4.1 Lack of anti-6-His antibody cross-activity with *E. coli* Top10 proteins 37
4.2 Expressed C-terminus protein of *un-24*^{PA} has multiple forms that are larger than expected in SDS-PAGE 37
4.3 Expressed protein of C-terminus cysteine mutants of *un-24*^{PA} have multiple forms, influenced by each of the cysteines 47
4.4 Effect of deletion of the last twelve amino acids of C-terminus protein 57

5. Discussion 65

6. Future studies 69

7. References 70

LIST OF FIGURES

1.1	Picture of self-incompatible colonies in DNA transformation plate.....	7
1.2	Comparison of pre-, post-escape, and wild type strains and cells by scanning electron microscopy and fluorescence microscopy.....	9
1.3	Mean time of escape in 10 subcultures each of 10 different transformants..	16
1.4	Western blots of self-incompatible extracted proteins.....	22
1.5	Model of incompatibility mechanism by large subunit of Ribonucleotide reductase in *N. crassa*.....	24
4.1	Western blot using anti-6-His antibody against protein from Top10 cells...	39
4.2	Replica samples of amplified PCR products of $un\text{-}24^{PA}$ cDNA by un-24FWPA and un-24RVPA primers.....	41
4.3	Nuclotide and amino acid sequence of PAccc clone.....	43
4.4	Western blot of PAccc purified protein.....	45
4.5	PCR-amplified 3800 bp product of PAccc plasmid using two different concentrations of DNA template and PAgcc primers.....	49
4.6	Nucleotide and amino acid sequences of PAccc and derivative cysteine mutant constructs.....	51
4.7	Western blot of single mutant constructs of PAccc purified protein.....	53
4.8	Western blot of double mutant constructs of PAccc purified protein.....	55
4.9	Western blot of PAggg and PAgc-deletion proteins.....	59
4.10	Nucleotide and amino acid Sequence of PAgc-deletion.....	61
4.11	Comparison of band sizes and patterns of PAccc and all the derived forms mutant.....	63

LIST OF TABLES

1.1 Characteristics of self-incompatible and compatible strains..... 11

3.1 Sequence of primers used for PCR and rolling circle mutagenesis 31

INTRODUCTION

Neurospora crassa Shear and Dodge is an Ascomycete fungus that is considered as "model system" because it is easy to grow and has a well-developed genetic system, individually a complete genome sequence. *N crassa* grows as a network of multinuclear cells called a mycelium, that comprises tubular filaments called hyphae. During vegetative growth, the hyphae grow by tip extension and branching, and hyphal fusion (anastomosis) occurs frequently within the interior of the colony for the purpose of communication and maintaining homostasis (Glass *et al.*, 2000; Xiang and Glass, 2002; Espagne *et al.*, 2002). Two genetically distinct isolates can also undergo hyphal fusion to form a heterokaryon, a cell containing genetically distinct nuclei. The presence of genetically different nuclei in the same cell may trigger a phenomenon called heterokaryon incompatibility (Smith *et al.*, 2000), a type of nonself recognition that leads to Programmed Cell Death (PCD). This nonself recognition system is thought to restrict heterokaryosis in fungi in nature and thus reduce the risk of transmission of deleterious genetic elements such as parasitic organelles, viruses and plasmids (Debets and Griffiths, 1998; Cortesi *et al.*, 2001; Biella *et al.*, 2002; reviews in: Glass and Kaneko, 2003; Micali and Smith, 2006). In fungi, this self-defense system may also be important for establishment and maintenance of territoriality by fungal individuals. Nonself recognition is likely a basic characteristic of all life forms that is, overall, poorly understood. Nonself recognition in fungi is experimentally tractable, and may provide general insights into the genetic and biochemical basis of the phenomenon. The PCD process in incompatible heterokaryons occurs through a series of steps involving a degenerative process of the fusion cell and often neighboring cells (Biella *et al.*, 2002). The PCD process usually

initiates by increases in the number and size of vacuoles (vacuolization) followed by cytoplasmic granulation. Then, the cytoplasm pulls away from the interior of the cell wall (cytoplasmic shrinkage) and becomes more condensed (condensation) until it becomes a small mass of material in the centre of the cell. Jacobson *et al.* (1998) also reported organelle degradation and disorganization as early steps of program cell death of a heterokaryon. Septa are plugged to inhibit spreading of incompatible nuclei and the lethal reaction to adjacent cells (Saupe *et al.*, 2000; review in Perkins, 1988; Jacobson, *et al.*, 1997). These processes cause cell death and compartmentalization of an incompatible heterokaryon (Marek *et al.*, 2003; Pinan-Lucarre *et al.*, 2003; review in Hamann *et al.*, 2008). Only, some of the heterokaryotic cells survive, but they exhibit abnormal morphology and reduced growth rates (Wu and Glass, 2000; review in Perkins, 1988). These cells are called self-incompatibles (SI), which grow very slowly for days to months, but suddenly convert to the wild-type-like growth form. This transition from inhibited to near-normal morphology is called "escape" from heterokaryon incompatibility (Smith *et al.*, 1996).

HETEROKARYON INCOMPATIBILITY LOCI

Heterokaryon incompatibility is genetically regulated during both the sexual and vegetative phases of the life cycle of fungi (Glass and Kuldau, 1992; Loubradou *et al.*, 1999). During the sexual phase, products of the mating-type locus regulate heterokaryon formation and mating compatibility (Deleu *et al.*, 1993; Staben and Yanofsky, 1990). Only isolates that differ at the mating type locus can form a heterokaryon in the brief

phase prior to karyogamy and meiosis (Saupe, 2000; Shiu and Glass, 1999; Haidari, 2002).

During the vegetative phase of the life cycle, vegetative incompatibility results upon fusion of two individuals that differ at any of their *het* or *vic* loci (for heterokaryon or vegetative incompatibility loci, respectively) (Kaneko *et al.*, 2006). In *N. crassa*, at least 11 loci control heterokaryon incompatibility function (Saupe *et al.*, 1996; Saupe and Glass, 1997). Each *het* locus in *N. crassa* has two or three alleles. Unlike in most systems, in *N. crassa* the mating-type locus also acts as an incompatibility locus during vegetative growth. During the sexual cycle, however, *tol*, a gene required for mating type vegetative incompatibility (Xiang and Glass, 2004) is turned off, and vegetative incompatibility is suppressed. Mutations have been isolated in *tol* that suppress mating-type-associated vegetative incompatibility, but do not affect incompatibility triggered by the other vegetative incompatibility loci (Leslie and Yamashiro, 1997).

All *het* loci in *N. crassa* appear to behave as allelic incompatibility factors (Saupe, 2000). Allelic incompatibility involves interaction between allelic forms of the same *het* locus, whereas non-allelic incompatibility involves specific allelic combinations at different *het* loci (Pál, 2005). The situation in *N. crassa* is in contrast to the non-allelic incompatibility common in *Podospora anserina*, another Ascomycete that is closely related to *Neurospora*. For example, the *het-c* locus of *P. anserina* is involved in nonallelic incompatibility through specific allelic combinations of *het-c*/*het-e* and *het-c*/*het-d* (Espagne *et al.*, 2002). An interesting example of an allelic incompatibility factor in *P. anserina* is the *het-s* gene, which has two alternative alleles, *het-s* and *het-S*, which differ only by 13 amino acids. *het-s* exhibits two phenotypes; [Het-s] represents a prion

that forms higher-order elongated fibrillar aggregates with an amyloid structure that is resistant to proteolysis (Balguerie *et al.*, 2003, 2004; Coustou-Linares *et al.*, 2001), and [Het-s*] occurs as a soluble, non-prion form. [Het-s] amyloids are associated with a highly flexible C-terminus domain of the protein, which is also responsible for prion propagation (self-perpetuation) and incompatibility activity (Balguerie *et al.*, 2003; Balguerie *et al.*, 2004). Co-expression of the two alleles of [Het-s] (in the prion state) and [het-S] in the same cell, causes lethal aggregates and triggers a cell death reaction. This toxicity is thought to be due to disruption of the formation of HET-s fibrillar prion to a more toxic intermediate form by incorporation of HET-S protein (Saupe, pers. com.).

Among all the incompatibility loci characterized from *N. crassa*, *het-6* causes one of the most intense heterokaryon incompatibility reactions. *het-6* was mapped to a 250-kbp region of the left arm of linkage group II (Smith *et al.*, 2000, 2006) and subsequently characterized at the molecular level. Vegetative incompatibility associated with the *het-6* locus is mediated by two closely linked genes, *het-6* and *un-24*, each of which comprise two allelic forms, designated as Oak Ridge (OR) and Panama (PA) (Smith *et al.*, 2000). Both genes act through an allelic mechanism, however, *het-6* and *un-24* are inherited as a block, therefore only un-24^{PA} *het-*6^{PA} *and un-*24^{OR} *het-*6^{OR} exist in the nature (Mir-Rashed *et al.*, 2000). *het-6* contains a conserved domain that is found in at least three other incompatibility genes in *N. crassa* and *P. anserina,* and that occurs as a repetitive element in the genomes of several filamentous fungi. *un-24* encodes the large subunit of ribonucleotide reductase (RNR), which plays the essential role of converting ribonucleotides to deoxyribonucleotides (Elledge *et al.*,1993*)*. This conversion is

required for de novo synthesis of DNA. The additional nonself recognition function of this enzyme in *N. crassa* has not been reported in any other organism.

The OR and PA alleles of UN-24 differ at 33 of the 113 amino acid positions at the C-terminus including a six amino acid insertion/deletion in this region and it is this C-terminus region that is implicated in both incompatibility activity and specificity (Micali and Smith, 2006; Wellman *et al.*, unpublished). These studies are aided by two methods for generating *un-24*^{OR}/*un-24*^{PA} partial diploids that are self-incompatible (SI). First, SI partial diploids can be made by crossing a wild-type PA strain to an OR strain that has the *het-6* locus (including *un-24*) as part of a segmental translocation. The second method is through transformation of *un-24*^{PA} DNA into an *un-24*^{OR} strain. According to Micali and Smith (2006), transformation of *un-24*^{OR} DNA into *un-24*^{PA} background resulted in strong incompatibility activity and recovery of no transformants because of cell death, however SIs that grew slowly and with an aberrant morphology were recovered when *un-24*^{PA} DNA was transformed into *un-24*^{OR} background.

CHARACTERISTICS OF SI TRANSFORMANTS

After DNA transformation of *un-24*^{PA} into *un-24*^{OR} strains, SI transformants appear on transformation plates as small star-shaped colonies compared to cloud-shaped self-compatible or wild-type colonies. These SI colonies can be recovered by subculturing to fresh medium where they are characterized by: 1) slow colony growth rate, 2) aberrant "flat" aconidiate morphology, and, 3) subsequent escape to near wild-type growth rate and form (Figure 1). From studies I carried out during this thesis

research (Siahbazi and Smith, unpublished), some detailed observations were made of self-incompatible characteristics that are explained in the following paragraphs.

As shown in Figure 2, *un-24*^{OR}/*un-24*^{PA} self-incompatible hyphae have shorter inter-branch lengths. The branch hyphae arise from the main hypha at an angle of about 90°, compared to about 45° for wild-type or escape branches. The SI colonies grow at about 1/10 of the rate of a compatible colony and neither aerial hyphae nor conidia are produced in abundance by SI colonies, in contrast to compatible colonies and escapes. There are also significant differences in cell volume of the SI transformants from control cells. Figure 2 illustrates that cell size in a SI hypha is much smaller than that of a post-escape or wild-type cell. The mean number of nuclei per cell observed in SI cells was almost 1/4 that of compatible cells. In addition, significantly more RNA was obtained from post-escape strains per gram wet-weight of mycelium than for SI strains. These differences and others are summarized in Table 1.

Overall, in comparison to SI strains, wild-type and post-escape strains are very similar in having tubular, well-extended hyphae with sharp branch angles. Aerial hypha, conidia and numbers of nuclei in each cell are all more abundant in both post-escape and wild-type colonies than in SI strains. All of these data demonstrate how the morphological characteristics of self-incompatibles are significantly different from wild type and post-escape strains.

FIGURE 1. Top, DNA transformation of PλBP/C (contains hyg^R and *un-24*^{PA}) into C9-2 (OR- background) gives small self-incompatible *un-24*^{OR}/*un-24*^{PA} colonies. Bottom left, when self-incompatible colonies are transferred, they grow slowly for about 4-7 days (i) and then escape (e) to near wild-type growth as shown schematically at bottom right (reproduced from Micali and Smith, 2005).

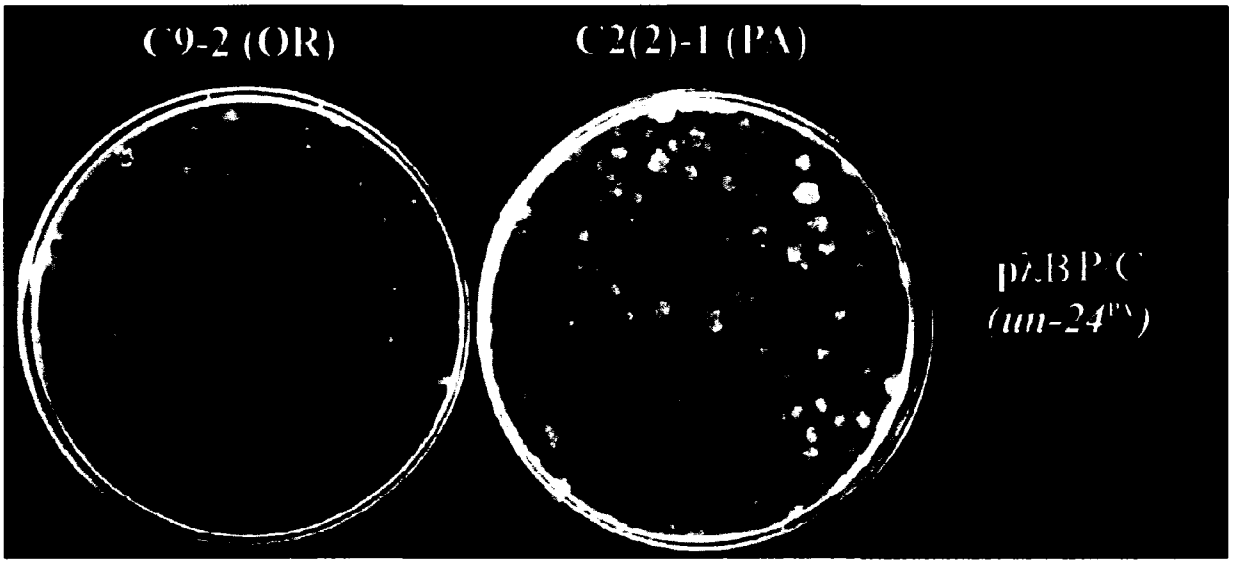
C9-2 (OR)
C2(2)-1 (PA)
pABPC
(un-24PA)

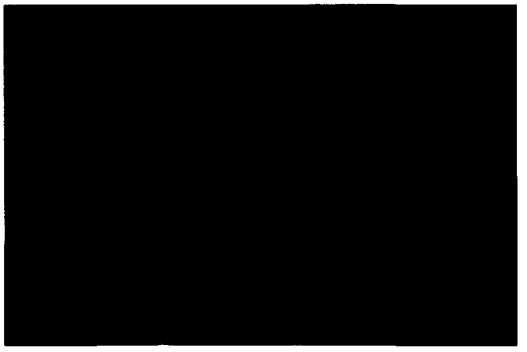

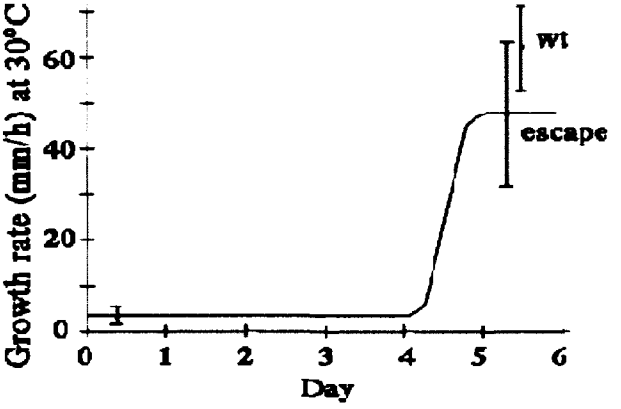
Growth rate (mm/h) at 30°C
60
40
20
0
0
1
2
3
4
5
6
Day
wt
escape

Figure 2. Comparisons of pre-escape, post-escape and wild type strains and cells. Left, scanning electron microscopy (panels A, C and E) and fluorescence microscopy following nuclear (DAPI) and cell wall (Calcofluor White) staining (panels B, D and F) comparisons of self-incompatible (A and B), post-escape (C and D), and wild-type colonies (E and F). The post-escape strain shown in panels C and D is from the same SI shown in panels A and B, consisting of a C9-2 (*un-24*^{OR}) strain expressing hygunPA, a fusion of hygR gene and the C-terminus of *un-24*^{PA}. The wild-type colony shown in panels E and F is strain C9-2 transformed with hygR vector pCB1004.

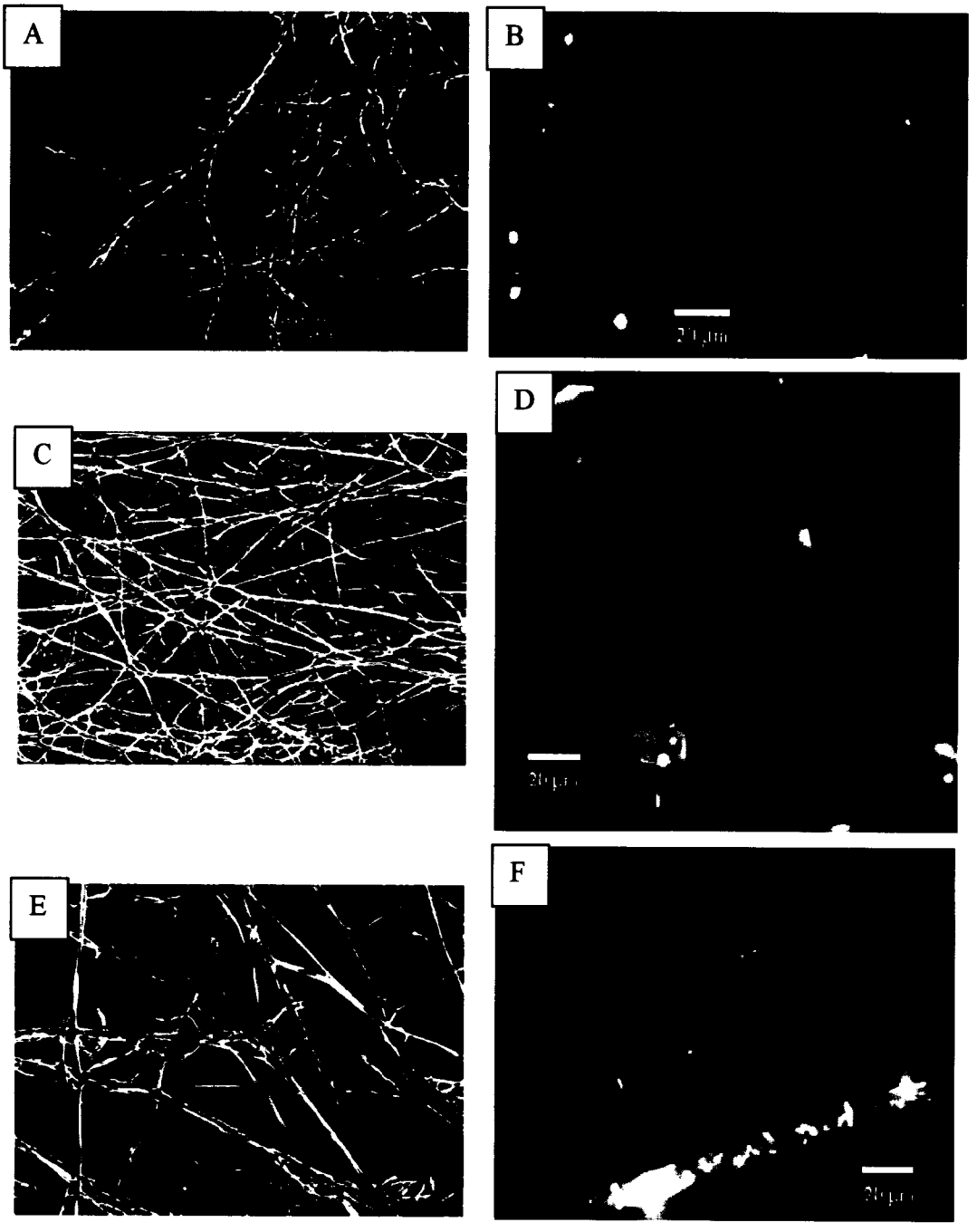
A
B
C
D
E
F

Table 1. Comparisons of SI strains and their post-escape forms (Siahbazi and Smith, unpublished). The post-escape form is not markedly different from wild-type form.

Characteristic	SI colony	Post-escape colony
Average growth rate	< 5 mm/h	> 40 mm/h
Branching length	short	long
Average branching angle	90°	45°
Average cell volume	300 μm^3	2000 μm^3
Mean number of nuclei/ cell	7	30
Presence of aerial hypha and conidia	_	+
Average RNA yield	85 ng/ µl	1110 ng/ µl

ESCAPE FROM HETEROKARYON INCOMPATIBILITY AND MECHANISM

The above observations were done to compare morphological characteristics of SI, escape and control (wild-type) colonies in order to understand the mechanism of escape in SI colonies. Escape is a phenomenon by which the slow-growing self-incompatible colony suddenly increases its growth rate to about wild type rates. According to Smith *et al.*, (1996), from 400 slow-growing, self-incompatible partial diploids, 80 escaped to the PA phenotype (i.e. the ectopic duplicated region was deleted) and 16 escaped to OR (the endogenous copy was deleted). Most of the escapes occurred at or shortly after day 20. In all cases the mechanism of escape from *het-6-un-24* self-incompatibility in segmental duplications was found to be through deletion of one or the other of the incompatibility genes (Smith *et al.*, 1996). These deletions centered on segments within the duplicated regions that contained *het-6* and *un-24* genes and this information was used to identify, clone and characterize these incompatibility genes. The results also demonstrated that the PA and OR DNA of deleted region carry reciprocal incompatibility activity (Smith, 2000). In another study with *N. crassa* by Xiang and Glass (2004), in addition to similar deletions, chromosomal rearrangements were detected in strains that had escaped from *het-c* heterokaryon incompatibility. In *N. crassa* one of these mutations resulted in the identification of *vib-1*, mutations of which suppress incompatibility associated with heteroallelism at *het-c* and *mat* (Xiang and Glass, 2004).

Characteristics of escape in over one hundred $un\text{-}24^{OR/PA}$ self-incompatible colonies that were generated by transforming the PA allele into an $un\text{-}24^{OR}$ strain have been observed in our laboratory to reveal a consistent trend. In contrast to previous demonstrations of escape involving deletion and rearrangement mutations, the *un-*

24^{OR}/*un-24*^{PA} self-incompatible colonies derived through transformations escape more rapidly (usually within 4-7 days) and at a much higher frequency (nearly all escape). The mechanism of escape from *un-24* incompatibility does not involve deletion, as was demonstrated by Micali and Smith (2006). In their study, Southern and PCR analyses were used with DNA extracted from post-escape colonies to show that, in most cases, post-escape colonies maintained both OR and PA forms of *un-24*.

Several studies in our laboratory have been performed to find out if there is a correlation between escape time and transgenic location, growth rate, or colony size. Figure 3, shows the measured mean time of escape in 10 subcultures of each of 10 individual transformants. These measurements indicated that separate subcultures of a given transformant have very similar escape times and that different transformants can have different escape times. Therefore, escape time appears to be influenced by the position of the transgene insertion within the genome, a factor that would vary from transformant to transformant. Measured pre-escape growth rates showed that there is no correlation between pre-escape growth rate and the time of escape. Therefore, escape does not appear to be influenced by number of cell divisions. Escape does appear to occur when the colony achieves a certain size, after a defined growth period. This feature has useful application because a small subculture of a pre-escape self-incompatible colony can be transferred prior to escape and maintained as self-incompatible.

The observed high frequency and rapid escape of *un-24*$^{OR/PA}$ SI colonies does not correspond to expectations, nor previous observations, of a mutation mechanism. Escape through deletion of one allele, or mutation in a suppressor gene are documented to be quite rare and stochastic (Smith *et al.*, 1996; Xiang and Glass, 2002). Recently, we

investigated the possibility of nuclear segregation as another possible escape mechanism. During hyphal growth, it is possible that cells could lose transformed nuclei through cell divisions. Escape may occur when a daughter cell has lost a transformed nucleus. However, this mechanism does not explain escape by hygunPA SI transformants. In this case, the 3' end of the hygromycin B resistance gene was fused to the 5' end of the *un-24*^{PA} C-terminal region with incompatibility function (Wellman *et al.*, unpublished). When transformed into an *un-24*^{OR} strain, this construct provides hygR function but also causes incompatibility. Such hygunPA SI transformants can, nevertheless, escape on hyg-containing medium. Deletion of the hygunPA construct is not possible since this would cause inhibition by hygromycin B in the medium. Deletion of the endogenous *un-24*^{OR} segment is also not possible since it provides the essential function of providing DNA precursors. This result was supported further when it was also shown that escape does not happen through decreases in copy number of either the transgene (carrying the PA alleles) or the endogenous OR copy (Siahbazi and Smith, unpublished).

Other possibilities that may explain the mechanism of escape by *un-24*$^{OR/PA}$ SI colonies include methylation and RNA interference (RNAi), both of which could modulate the transcription of either the transgene or the ectopic segment. Studies done by Saeed and Smith (unpublished) showed that a methylation deficient strain (*dim-2*) escapes at the same rate and timing as SI in a *dim-2*$^{+}$ background. They concluded that methylation is not involved in escape. Further support for this conclusion came from semi-quantitative RT-PCR (Gibbs, 2004) and real-time quantitative PCR (Siahbazi and Smith, unpublished) to determine whether there were changes in transcription levels of the OR and PA alleles in SI strains prior to and after escape. Neither experiment provided

evidence that relative transcript levels changed for either the transformed copy or the endogenous copy upon escape.

RNA silencing was originally characterized in *N. crassa* as "quelling". It was observed to reduce expression of both the transformed sequence and the endogenous sequence that had identity to the transformed gene (Romano and Macino, 1992). However, studies done by Zymantas and Smith (unpublished), showed that quelling does not appear to be involved in *un-24*-associated escape. This is based on experiments with the quelling defective mutant, *qde-2*, which was shown to escape just as well as a *qde-2*$^{+}$ strain. These indications that escape by *un-24*$^{OR/PA}$ SI strains does not involve mutation, nuclear sorting, changes in transcription levels or RNA silencing has led us to explore post-translational processes that might account for escape.

Figure 3. Mean time of escape in 10 subcultures each of 10 different transformants (M1 - M10) indicates there is an interaction between the location of ectopic copy and time of escape.

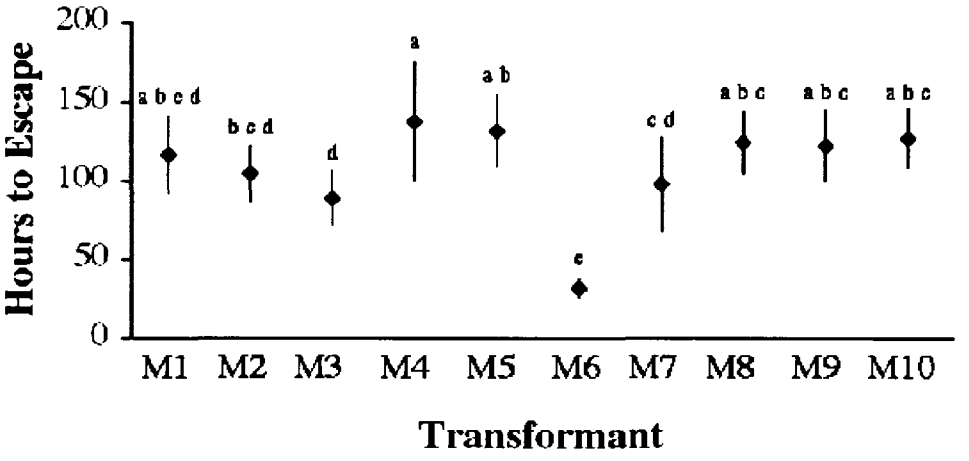

Transformants not connected by same letter are significantly different (LSMeans Differences Tukey HSD)

RIBONUCLEOTIDE REDUCTASE (RNR)

At least two mechanisms could account for the dramatic morphological changes that are associated with *un-24*-associated incompatibility: the incompatibility could be the result of a toxic heterodimer of the large subunit ribonucleotide reductase, or could result through malfunction of the heterodimer complex, and perturbation of nucleotide abundance and/or ratios. To elaborate on these two mechanisms a review of relevant literature on RNR is provided in the following section.

The gene *un-24* of *N. crassa* encodes the large subunit of type I ribonucleotide reductase, RNRL (Smith *et al.*, 2000). Among three classes of RNR, the type I RNRs are found in all the eukaryotes, some viruses and some prokaryotes like *E coli*, and differ from type II and III RNRs by having a diiron-oxygen cofactor (reviews in: Fontecave, 1998; Wellman *et al.*, unpublished; Kolberg, *et al.*, 2004). The type I ribonucleotide reductase is an evolutionarily conserved enzyme which catalysis the reduction of ribonucleotides to their corresponding deoxyribonucleotides and is therefore essential for DNA replication and repair (Bleifuss *et al.*, 2001; Eriksson *et al.*, 1997; Peter, 2002). The RNR holoenzyme is a tetramer composed of two large subunits, R1, and two small subunits, R2 (Figure 5; Eriksson *et al.*, 1997; Lee and Elledge, 2006; Booker *et al.*, 1994). The active site of the enzyme is located on the R1 subunit. R1 also contains two allosteric sites that regulate substrate specificity and enzyme activity (Wellman *et al.*, unpublished; Kasrayan *et al.*, 2004; Uhlin and Eklund, 1994). There is a dinuclear iron centre and tyrosine residue in R2 which is deeply buried within the protein (Xu *et al.*, 2006; review in: Fontecave, 1998). In the active RNR, this dinuclear iron centre generates a stable tyrosil radical to initiate the reduction reaction (Lin *et al.*, 1987; reviews in:

Ekland *et al.*, 2001; Mulliez *et al.*, 1993; Nordlund and Eklund, 1993; Kolberg *et al.*, 2004). The tyrosil radical in R2 generates a thiyl radical (HS-SH) of the cysteines of the R1 subunit (C439 in *E coli*) via a long-range proton-coupled electron transfer, which abstracts the 3' hydrogen atom of NDP substrate (Persson *et al.*, 1998; review in Ekland *et al.*, 2001). The NDP is reduced by transferring a hydrogen atom from redox active cysteines of R1 (C225 and C462 in *E coli*) to 2' hydroxyl of the ribose sugar, which leaves as a water molecule (review in: Fontecave, 1998). In this stage, a disulfide bond is formed (S-S) between cysteines in the active site (Mao *et al.*, 1992*)*. This active-site disulfide is reduced by another pair of cysteines located in the C-terminus region (C754 and C759 in *E coli*). This C-terminus forms a flexible arm that swings into the R1 catalytic pocket for disulfide interchange and then swings back to get reduced by glutaredoxin or thioredoxin (Aberg *et al.*, 1989; Wellman *et al.*, unpublished; Mao *et al.*, 1992).

PROPOSED INCOMPATIBILITY MECHANISM OF *un-24*

Interesting observations were made recently that may explain both incompatibility function and provide insights into the mechanism of escape. Haidari (2002) used Western blots and anti-mouse-RNR-N to show that protein aggregation is associated with *un-24* incompatibility. Lane 2 of Figure 4a shows a band of 103 kDa, the predicted size of the large subunit of ribonucleotide reductase (UN-24) from *N. crassa*. Proteins of *un-24*$^{OR/PA}$ self-incompatible colonies were denatured and loaded in order of most inhibited (lane 3) to least inhibited (lane 7). The anti-mouse RNRL antibody revealed a high molecular weight protein of about 200 kDa in proteins from SI colonies in lanes 3 - 6, the intensity of which was approximately correlated with growth rates of the SI colonies. In lane 7, representing the fastest growing SI strain examined, an intense pair of bands of the expected size for UN-24 is seen. This strain may represent a SI that had recently undergone escape from incompatibility. These observations suggest that SI is associated with formation of a non-reducible complex of UN-24^{OR}–UN-24^{PA}, and that escape involves the break-down of this complex. In a follow-up study it was observed that expression of a flag-tagged C-terminus portion of UN-24^{PA} appeared to undergo proteolytic cleavage upon escape (Figure 4b; Arzhangi and Smith, unpublished). Small, relatively low molecular weight fragments were observed in post-escape colonies but not in their pre-escape counterparts. This information suggests a model in which *un-24*-associated SI is mediated by heterodimeric protein complexes.

Additional studies by Wellman and others in our laboratory have characterized some key regions of *un-24* that are involved in incompatibility, as follows. Catalytic activity by UN-24 requires the entire protein. Incompatibility specificity is associated

with the C-terminal region, that differs significantly between the OR and PA allelic forms. Only 60 amino acids of the *un-24*^{PA} protein (amino acids 861-920) are required for PA-specific activity but nearly the full length of *un-24*^{OR} (129-929) was required to trigger incompatibility activity. Conserved cysteines in the C-terminus of both allelic forms were also found to be essential for incompatibility function. Based on size-exclusion chromatography and Western blotting, the PA C-terminal tail binds in a non-reducible manner to the *un-24*^{OR} protein. Strong reducing and denaturing conditions were not able to break this interaction. The model proposed (Figure 5) accounts for these observations and those of the catalytic mechanism of RNR as discussed above.

Figure 4. A) Western blot experiments provide key insights into the *un-24* incompatibility mechanism. A) Anti-mouse RNRL antibody was used in Western blots of mouse protein (lane 1) and protein from OR strains of *N. crassa* that were untransformed (lane 2), or self-incompatible (lanes 3-7) transformants. The results indicate that a protein complex is associated with *un-24* incompatibility and that escape may involve the break-down of this complex (Haidari 2002). **B)** Detection of hygflagunPA protein with anti-flag antibodies reveals small protein fragments (2A & 2B) in post-escape but not pre-escape colonies (1A & 1B). This suggests that the flag-tagged hygunPA protein is undergoing proteolytic cleavage during the escape process (Arzhangi and Smith, unpublished).

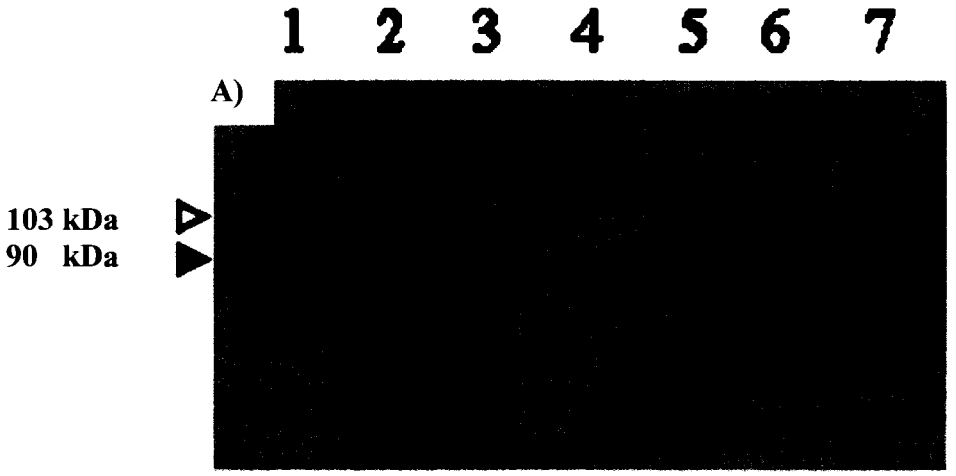
1 2 3 4 5 6 7
A)
103 kDa
90 kDa

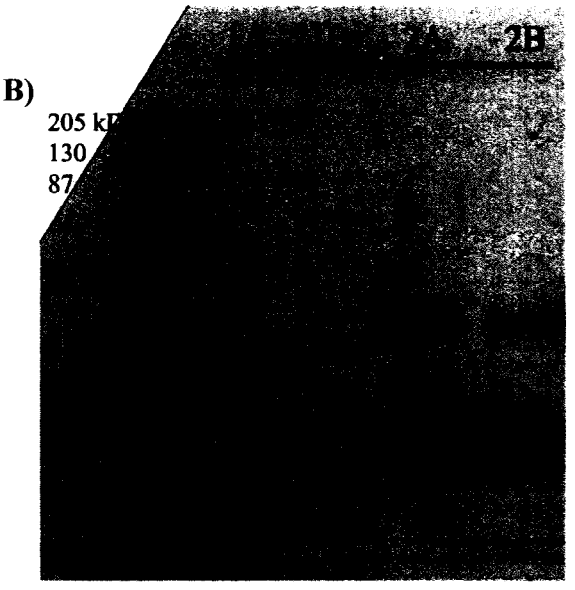
2B
B)
205 kD
130
87

Figure 5. Top, Schematic of ribonucleotide reductase holoenzyme. The enzyme comprises two large subunits (RNR1) and two small subunits (RNR2). The C-terminus arms with three conserved cysteines are shown at the top. **Bottom,** Model of incompatibility mechanism by large subunit of ribonucleotide reductase in *N. crassa*. The small subunit dimer that is part of the RNR holoenzyme is not shown. A) In a self-compatible system, the conserved redox-active cysteine pair on the C-terminal flexible arm transfers reducing equivalents from glutaredoxin (GR) or thioredoxin (TR) to the cysteine pair in the catalytic pocket. The flexible arm of one monomer moves into the catalytic site of the other monomer in the homodimer and disulfide interchange occurs. This leads to the regeneration of the catalytic cysteine pair and another round of product turnover. B) In a self-incompatible system, regeneration of the cysteine pair in the catalytic pocket is halted when the cysteine pair on the flexible arm of the PA monomer (black) interacts with the cysteine pair in the catalytic pocket of the OR monomer (grey). Improper disulfide interchange leads to irreversible binding of the two monomers (Wellman *et al.*, unpublished).

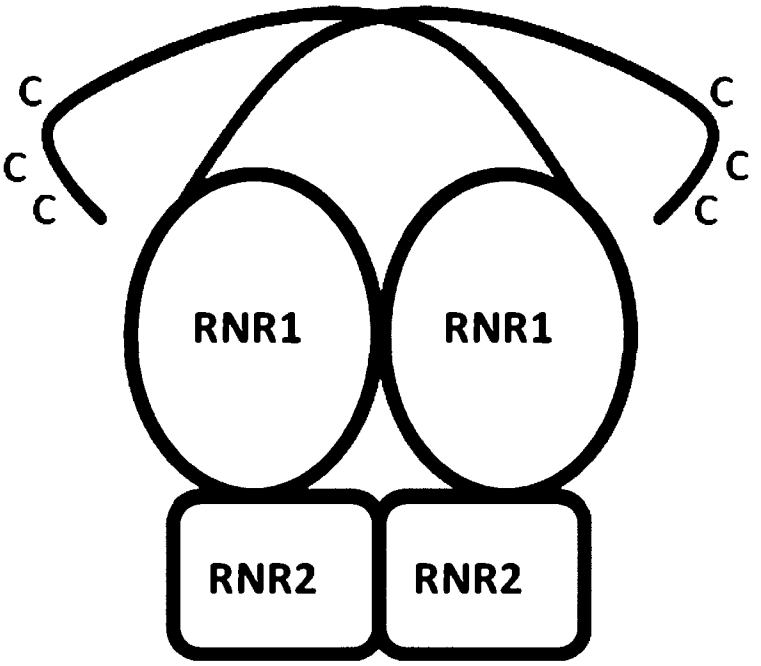
C
C
C
C
C
C
RNR1
RNR1
RNR2
RNR2

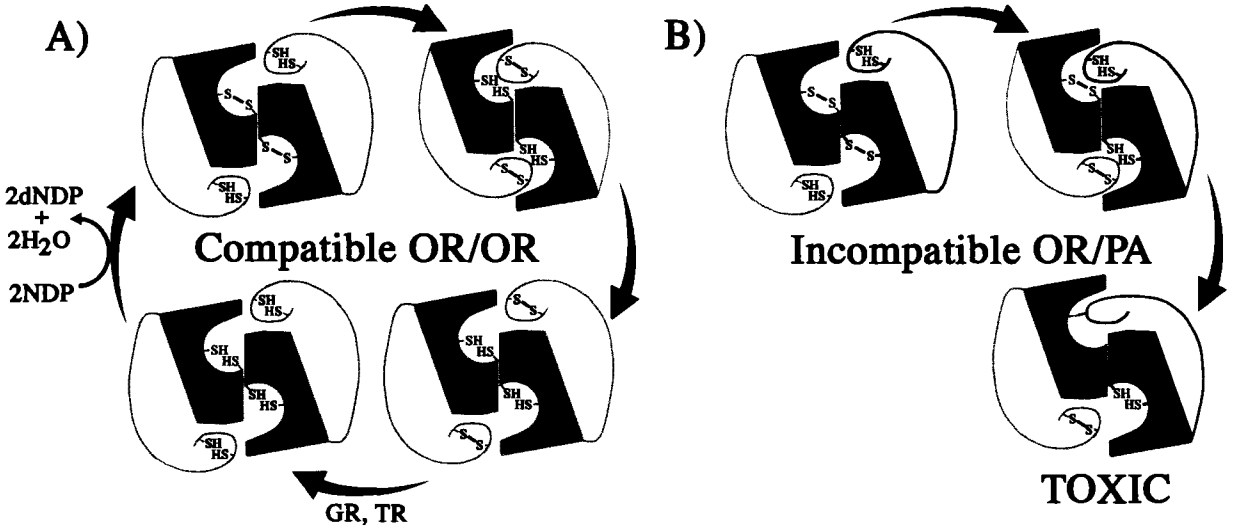
A)
2dNDP
+
2H2O
2NDP
Compatible OR/OR
GR, TR
B)
Incompatible OR/PA
TOXIC

OBJECTIVES

In this thesis, I investigate the electrophoretic mobility of the C-terminal region of the *un-24*^{PA} protein that was expressed in *E. coli*. I found evidence that *E. coli* modifies this expressed protein, resulting in reduced mobility and multiple forms of the protein under standard SDS-PAGE conditions. Second, I constructed and expressed several cysteine substitution mutants of this C-terminus region and used SDS-PAGE banding patterns to infer the role of disulfide bonds in the complex banding pattern. In the future, these proteins can be used to generate antibodies that are specific to the PA allele C-terminal region and for further biophysical investigations. The work also sets the stage for *in vitro* analysis of protein–protein interaction studies of this interesting incompatibility factor.

MATERIALS AND METHODS

un-24 constructs, microbial strains and growth conditions

Template DNAs used in initial PCRs included hygunPA and hygunPAgcc (Wellman *et al.*, unpublished). The construct designated as hygunPA contains the hygromycin B- resistance gene fused in-frame to the last 405 bp of coding region of *un-24*^{PA} cDNA all cloned in the plasmid pCR2.1. Also in pCR2.1, the construct hygunPAgcc contains the same *un-24* region but has the first cysteine (most N-terminal) codon mutated to a glycine codon. Vectors pQE31 and pQE30UA (Qiagen, Mississauga, Ontario) were used to express the DNA fragment of interest. Both vectors provide for a 6-histidine tag on the N-terminus of the expressed protein. Plasmids were amplified in One-Shot Top10 *E. coli* chemically competent cells (Invitrogen,

Mississauga, Ontario) overnight at 37 °C and 250 rpm in LB liquid (no agar) or LB agar medium (1.5% agar), containing 100 μg/ml Ampicillin. Plasmid DNAs were obtained by Wizard plasmid miniprep (Promega, Nepean, Ontario). Bacterial glycerol stocks of each plasmid were prepared and stored at -80 °C.

Primers and PCR amplifications

Primer sequences used in this study are given in Table 2. Primers un-24FWPA and un-24RVPA were used to PCR amplify 306 bp of the C-terminus coding region using hygunPA as a template. The product was first cloned into a TA-cloning vector and then ligated in frame with the 6-His tag of the vector pQE31 using the *Bam*H1 and *Sal*I sites in the respective primers as described below. In order to obtain high specificity in PCR products, annealing temperatures of 48, 50, 52, 54, 56, and 58 °C were tested. The optimal primer annealing temperature was found to be 54 °C and subsequent PCRs used this annealing temperature. PCR reactions were conducted in a total volume of 20 μl. The master mix was prepared by adding 2 μl of 10 μM of each primer, 2 μl template DNA (1-2 ng/μl), 0.4 μl of dNTPS (100mM), and 0.2 μl of DNA Taq polymerase (Bioshop, Burlington, Ontario) for each reaction. Reactions were initiated with 5 minutes incubation time at 94 °C followed by 30 cycles at 94 °C for 1 min (denaturation), 54 °C for 30 s (primer annealing), and 72 °C for 35 sec (elongation). PCR products were analyzed by agarose gel electrophoresis and ligated into vector pCR 2.1-TOPO according to the vector manufacturer instructions (Invitrogen). This construct was called "PATOPO" and verified by PCR and restriction digestion and then sequencing.

Three µg of cloned PATOPO DNA was cut in a 50 µl digestion reaction by adding 3.5 µl of each *Bam*H1 and *Sal*I restriction enzyme (New England Biolabs, Pickering, Ontario), 3.5 µl of BSA, and 5 µl of NEB buffer 3 and incubated overnight. The digested DNA was run on a 0.8% agarose gel and desired band of 320 bp was excised. The excised band was purified from the gel by addition of 750 µl of NaI (6 M) and incubation at 58 °C for about 5-10 min prior to addition of 12 µl of glass milk. After a brief vortex the tube was placed on ice for 30 min, followed by centrifugation at 16,100 x g for one min. The supernatant was discarded and 750 µl of -20 °C wash buffer (50 mM NaCl, 10 mM Tris, pH 7.6, 2.5 mM EDTA, 50% ethanol) was added and the pellet was resuspended by gently vortexing. This wash step was repeated twice more followed by centrifugation, discarding the buffer and addition of 10 µl of autoclaved water to elute the pellet in a 50 °C water bath for 5 min. Following a brief centrifugation the supernatant (containing DNA) was transferred into a fresh tube to await the ligation step. The pQE31 vector was digested with *Bam*HI and *Sal*I, followed by electrophoresis, and the digested vector was gene-cleaned as described above. Insert and vector DNA were quantified by spectrophotometry and gel electrophoresis. Ligation were performed using 1 µl of 30 ng / µl and 10 µl of 10 ng / µl of recovered insert and vector DNA, respectively, according to the New England Biolabs protocol. The ligation reaction was incubated at 16 °C overnight and then transformed into *E. coli* Top10 chemically competent cells. Plasmids containing the correct inserts were verified by PCR using the un-24FWPA and un-24RVPA primers and restriction enzyme digestion, and then finally by sequencing. This final 306 bp fragment of the C-terminal coding region of *un-24*^{PA} cloned into pQE31 was designated as "PAccc". A similar procedure was used to clone

the last 310 bp from hygunPAgcc except that the un-24FWPA and un-24RVPA PCR product was ligated directly into the TA cloning expression vector pQE30UA (Qiagen), by which we obtained the PAgc clone, with a deletion of the last 12 amino acids containing the third cysteine (PAgc). The PAgc clone was also verified by DNA sequencing.

Rolling circle site - directed mutagenesis

The PAccc plasmid was used as a template to obtain additional cysteine mutants in the C-terminal region. For this purpose, a few sets of forward and reverse oligonucleotide primers were designed and PAGE purified according to the Stratagene QuickChange Site-Directed Mutagenesis protocol (Stratagene, Mississauga, Ontario). One or more cysteine codons were substituted to glycine codons in both forward and reverse primers, by changing the codon tgc to ggc. Single mutation constructs of PAgcc, PAcgc, and PAccg were obtained using PAgcc, PAcgc, and PAccg forward and reverse primers, respectively (Table 2). The procedure used was adapted from the Stratagene QuickChange Site-Directed Mutagenesis kit instructions. PCR annealing temperatures were determined by performing temperature-gradient PCR reactions. The standard PCR reaction was conducted in a total volume of 50 µl. Master mix was prepared by adding 10 µl of PCR buffer, 1.25 µl of 10 µM of each primers, 0.2 µl template DNA (137 ng/µl), 0.4 µl of freshly mixed dNTPS (100mM), and 0.1 µl of Taq DNA polymerase (Bioshop). Different annealing temperatures of 65, 70, 75 and 80 °C were tested. Based on product yield, primer annealing temperature was optimal at 75 °C and all subsequent PCRs used this annealing temperature. PCR reactions were initiated with 3 min at 95 °C followed by

30 cycles at 94 °C for 30 s (denaturation), 75 °C for 30 s (primer annealing), and 72 °C for 4 min (elongation), followed by a final extension period at 72 °C for 6 min. The rolling circle mutagenesis reaction was performed with the same PCR procedure. Master mix was prepared on ice, by substituting 0.5 µl of iProof high fidelity DNA polymerase (Bio-Rad, Mississauga, Ontario), instead of Taq DNA polymerase, for each PCR reaction. A 2 min elongation time was applied to extend the entire ~3,800 bp plasmid. Ten µl of PCR product was run on an agarose gel to assure amplification of correct sized fragment and, at the same time, the amplification product was digested using 1 µl of *Dpn*I with NEB buffer 4 (New England Biolabs) at 37°C for one hour, to degrade parental plasmid dsDNA (which would not have the desired mutation). Ten µl of the *Dpn*I-digested PCR product was used to transform 50 µl of Top10 cells. Transformation was performed according to Invitrogen TopoTA cloning kit and the entire transformation reaction was spread onto four freshly made LB-ampicillin agar plates and incubated overnight at 37 °C. Four colonies of each constructs were sequenced to verify that the correct mutation was incorporated into each construct.

Using a similar rolling circle mutagenesis procedure, the double mutation constructs PAggc, PAgcg, and PAcgg were obtained using PAgcc, PAgcc, PAcgg forward and reverse primers with PAcgc, PAccg, PAccg template DNAs, respectively (Table 2). Finally, the triple mutation PAggg construct was obtained using PAgcc primers and the PAcgg DNA as template. All constructs were verified by DNA sequencing and glycerol stocks of strains carrying each of the above plasmids were prepared for long-term storage at -80 °C.

Table2. Sequence of the PCR primers used in this study. *Bam*HI and *Sal*I integrated sequences are shown in red capital letters. Substituted nucleotides for rolling circle mutagenesis experiments are presented as lower case red letters.

Primers	Sequences
	*Bam*HI
un-24FWPA	ACGGATCCTCCTGCTGAAGATTCTG
	*Sal*I
un-24 RVPA	CGGTCGACACCGCTGCACATAACGC
PAgccFW	GAGGTAGTCTCAgGCCCCTACGTTCCC
PAgccREV	GGGAACGTAGGGGCcTGAGACTACCTC
PAcgcFW	GATCCCTCCTCCgGCGTTATGTGCAGC
PAcgcREV	GCTGCACATAACGCcGGAGGAGGGATC
PAccgFW	CCTCCTGCGTTATGgGCAGCGGTGTCG
PAccgREV	CGACACCGCTGCcCATAACGCAGGAGG
PAcggFW	GATCCCTCCTCCgGCGTTATGgGCAGC
PAcggREV	GCTGCcCATAACGCcGGAGGAGGGATC

Protein expression assays

Over-expression of His-tagged proteins was performed by adding isopropyl-β-D-thiogalactoside (IPTG) to the bacterial culture medium. IPTG binds to the *lac* repressor protein and inactivates it. Therefore, the Top10 cell's RNA polymerase can transcribe the sequences downstream from the T5 promoter (The QIAexpressionist). To determine the appropriate IPTG concentration and protein expression time, several small-scale protein expression experiments were performed using 0.5, 1, and 2 mM of IPTG, and expressed proteins were analyzed after 0.5, 1, 2, and 3 hours and overnight culture. For this purpose, a single colony of the PAccc was inoculated into 7 ml of culture medium containing 100 μg/ ml ampicillin, and grown overnight. One-hundred ml of pre-warmed medium (including ampicillin) was then inoculated with 6 ml of the overnight culture and grown at 37 °C for 1.5-2 hours, with 225 rpm shaking, until the OD_{600} was 0.5-0.7. Fifteen ml of culture was centrifuged at 5,856 x g for 20 minutes and the pellet was kept at -80 °C as an uninduced control. For the remaining culture, expression was induced by adding a given amount of IPTG and incubated in 30 °C incubator, with 30 rpm shaking. 15 ml aliquots of culture were taken at times of 0.5, 1, 2, 3 hours and the last 15 ml left to grow overnight. All the samples were centrifuged immediately, and pellets kept at -80 °C until protein extraction. Four hundred μl of each of buffer A (100 mM NaH_2PO_4, 10 mM Tris, 6M GuHCl, pH 8) and buffer B (100 mM NaH_2PO_4, 10 mM Tris, 8 M urea, pH 8) were added to the pellets and vortexed gently to mix and thaw the pellets. Most proteins in inclusion bodies are solubilized with 8 M urea or 6 M GuHCl according to the QIAexpressionist fact sheet (Qiagen). The tubes were centrifuged at 16,100 x g for 20 min at 4 °C and supernatants were transferred into the fresh tubes. Five μl of 2x SDS-

PAGE sample buffer, 0.09 M Tris·Cl, pH 6.8; 20% glycerol; 2% SDS, 0.02% bromophenol blue; 0.1 M DTT, were added to the 15 µl of each sample and vortexed for a few seconds. Samples were heated for 10 min at 97°C, vortexed and then centrifuged for 10 s. Eighteen µl of uninduced and induced samples were loaded onto a 30% SDS-PAGE gel for analysis and Western blotting.

SDS polyacrylamide gel electrophoresis (SDS-PAGE)

To prepare SDS-PAGE gels, the glass plates were cleaned by ethanol and assembled. A 30% acrylamide gel was prepared using 4,800 µl of autoclaved dH_2O, 150 µl of autoclaved 10% SDS, 3800 µl of autoclaved Tris (1.5 M), 6,300 µl of 40% acrylamide/Bis- acrylamide (Bio-Rad), and 150 µl of 10% APS. Ten µl of TEMED (N, N, N', N'-Tetramethylethylenediamine, 99%, Sigma) was added and mixed well, prior to pipetting into the 8 x 10 cm x 0.75 or 1 mm thick glass plate gel apparatus (Bio-Rad). The gel was overlaid with dH_2O, and allowed to polymerize for 10-15 minutes. The water overlay was decanted from polymerized running gel before adding the stacking gel. Stacking gel was prepared by adding 4,060 µl of autoclaved dH_2O, 66.8 µl of autoclaved 10% SDS, and 1,660 µl of autoclaved Tris (1 M), 880 µl of 40% acrylamide, and 66.8 µl of APS (10%). TEMED (6.6 µl) was added just prior to application of the stacking gel to the running gel. Immediately following addition of the stacking gel the comb was inserted between the plates and the system was left to sit for another 15 min. The glass plate apparatus was placed in the electrophoresis chamber, filled with reservoir buffer (3 g Tris, 14 g glycine, and 1 g SDS, up to 1 L of dH_2O) and combs were carefully removed. Seven µl of precision plus protein kaleidoscope standard (Bio-Rad) and 18 µl of prepared

samples were pipetted slowly into separate wells. Electrophoresis was at 150 V for about 15 min or until protein standard markers were separated, and then the voltage was increased to 250 V for an additional 40 min. Gels were stained with Coomassie brilliant blue, or prepared for Western blotting.

Coomassie staining

For Coomassie staining, SDS-PAGE gels were fixed overnight in 10% acetic acid glacial and 25% methanol. Gels were then stained for two hours in filtered 25% Coomassie brilliant blue R, 50% methanol and 7.5% acetic acid with slow shaking. Gels were destained using several changes of 25% methanol and 10% acetic acid until a good contrast between bands and background was observed. Coomassie stained gels were washed with 7.5% acetic acid and dH_2O each for 1 hour and placed on the light box and photographed (Canon camera, power shot A85). Gels were stored for extended periods if needed in 7.5% acetic acid at 4 °C.

Western blot analysis and immunoblot detection

Following gel electrophoresis, the stacking gel was removed from running gel, and sandwiched between two Bio-Rad mini trans-blot filter papers, with a 0.45 μm Bio-Rad nitrocellulose membranes in front of each gel. The gel sandwich was transferred to a buffer-tank-blotting apparatus, filled with transferring buffer (Tris 3 g, glycine 14.4 g, methanol 200 ml up to 1 L dH_2O) and transferred overnight at 30 V. The next day the apparatus was disassembled, protein standard markers were marked by a fine pencil on the nitrocellulose membrane and membrane blocked with 5% fat-free dry milk in TBST

(3.152 g of Tris, 8.006 g of NaCl and 1 ml of Tween-20 up to 1 L dH_2O, pH 7.6) for 1.5 hour at room temperature, with a very slow shaking. The membrane was then incubated with 3 µl of primary antibody (1 in 7,000 dilution of Qiagen RGS-His antibody) in 20 ml of blocking solution for 1 hour at room temperature with very slow shaking. The membrane was then washed with TBST at room temperature and vigorous shaking for one hour, and then incubated with 3 µl of secondary antibody (Promega anti-mouse-HRP conjugate) in 20 ml of blocking solution for 1 hour at room temperature with very slow shaking. The membrane was then washed three times for 10 min each with TBST under vigorous shaking. A 1:1 mix of Sigma Chemiluminescent reagent and reaction buffer was prepared (700 µl in total) and applied to the membrane for 3-5 minutes. The membrane was enclosed in plastic wrap and exposed to the Kodak BioMax light film. Films were developed using Kodak developer and fixer.

Protein minipreps of 6xHis-tagged proteins under native condition

Two ml of overnight culture of bacteria, harboring recombinant plasmid, was used to inoculate 25 ml of pre-warmed LB liquid medium and left to grow for 1-2 hrs, at 37 °C and 225 rpm, to reach the OD_{600} of 0.5 –0.7. Expression was induced by adding IPTG (Bioshop) into the culture to a final concentration of 1 mM and incubated overnight at 30 °C and 30 rpm. Subsequent procedures were performed at 4 °C to avoid protein degradation. Cells were harvested by centrifugation for 20 min at 5,856 x g and supernatant was discarded. The pellet was resuspended in 5 ml of sonication buffer and gently vortexed with care to avoid frothing. Sonication buffer was prepared by filter sterilizing 5.5 µl of 1 M Tris, 0.5 µl of each 1 M $MgCl_2$ and Imidazole (Sigma, Oakville,

Ontario), 50 µl of 1M NaCl, 2 µl of Tween 20, up to 50 ml dH_2O (pH 7.2), and 1/8 of protease inhibitor cocktail tablets (Roche, Mississauga, Ontario) added just before use and kept at 4 °C. The tube with this mixture was placed on NaCl and ice to keep temperature low while sonicating and then sonicated 5 times with 20 sec pulses separated by 20 sec cooling, at 70% duty cycles and 4 output control (20 Hz) using sonicator (Sonics and materials, Inc. vibra cell). Cell lysate (1.5 ml) was transferred to a fresh microfuge tube and centrifuged for 20 min at 16,100 x g. Supernatant containing all the expressed protein was transferred to a fresh tube and 25 µl of Ni-NTA agarose resin (Qiagen) was added and gently mixed in the multipurpose rotator for 40 min. Ni-NTA agarose contains Ni-NTA which has high binding capacity to histidine residues. The Ni-protein pellet was washed two times in 100 µl of wash buffer (filter sterilized 5.5 µl of 1 M Tris, 0.5 µl of 1 M $MgCl_2$, 1 µl of 1M imidazole, 50 µl of 1M NaCl, 2 µl of Tween 20, up to 50 ml dH_2O, pH7.2, and 1/8 of protease inhibitor cocktail tablet) by centrifugation for 2 min at 16,100 x g. The protein was eluted by adding 100 µl of elution buffer (filter sterilized 5.5 µl of 1 M Tris, 0.5 µl of 1 M $MgCl_2$, 2.5 ml of 1M imidazole, 50 µl of 1 M NaCl, 2 µl of Tween 20, up to 50 ml dH_2O, pH7.2, and 1/8 of protease inhibitor cocktail tablet) to the pellet. The tube was centrifuged for 3 min at 16,100 x g and supernatant containing his-tagged protein was transferred into a fresh tube. The purified protein was analyzed directly by SDS-PAGE or stored at 4 °C. Protein purification under reducing conditions was performed by adding 0.1% BME and 1 mM urea to the sonication, wash, and elution buffers.

To make sure that there is no protein in the inclusion bodies, cell debris of the PAccc and Top10 cells were mixed with 8 M urea. For this purpose, 100 µl of 8 M urea

was added to the cell debris obtained from lysate after sonication, vortexed and heated for 10 min after adding 60 µl of loading buffer.

RESULTS

Lack of anti-6-His antibody cross-reactivity with* E. coli *Top10 proteins.

To make sure that no protein expressed from Top10 cells interferes with the protein of interest, expressed protein of Top10 cells that did not contain a 6-His-expression vector was immunoblotted. Figure 6 shows that anti-6-His antibody do not produce an immunoreactive band in Western blots of proteins from Top10 cells. In comparison, proteins from the cell debris of PAccc (described below) were solublized with 8 M urea to reveal a 20 kDa protein band that bound to the anti-6-His antibody.

Expressed C-terminus protein of* un-24^{PA} *has multiple forms that are larger than expected in SDS-PAGE.

The last 306 bp of the *un-24*^{PA} gene, encoding the C-terminus, was amplified by un-24PA forward and reverse primers (Figure 7) and cloned into the TA- vector. This vector was cut by restriction enzymes, and the insert was then ligated in-frame with the 6-His residues of the pQE31vector. Figure 8 shows the nucleotide and amino acid sequence of the PAccc clone. Figure 9 shows the Western blotting of the protein from PAccc expressed in Top10 cells. The same banding pattern was evident for PAccc protein in uninduced (data not shown) and induced samples with two bands of 20 and 18 kDa. However, a third band of 16 kDa appeared when proteins from induced cells were

extracted in the presence of BME and urea or BME and urea and DTT. Interestingly, the observed protein bands are all larger than the 13.2 kDa expected size for the PAccc protein. This predicted size is based on calculations using the Expasy program (http://ca.expasy.org/tools/pi_tool.html). Extractions with BME alone did not have this reducing effect on the PAccc purified protein. All the subsequent samples extracted under "reducing" conditions were treated with just BME and urea.

Figure 6 . Western blot using anti-6-His antibody against protein from Top10 cells that do not contain the 6-His vector. Shown in this image are, from right to left, total Top10 protein, Top10 protein purified using 6-His agarose beads, and solublized protein of the Top10 cell debris using 8M urea. None of these Top10 extracts were immuno-reactive with the anti-6-His antibody. In comparison, the most left lane in the figure is of a 20 kDa protein band from extracts of solublized cell debris of PAccc-expressing Top10 cells.

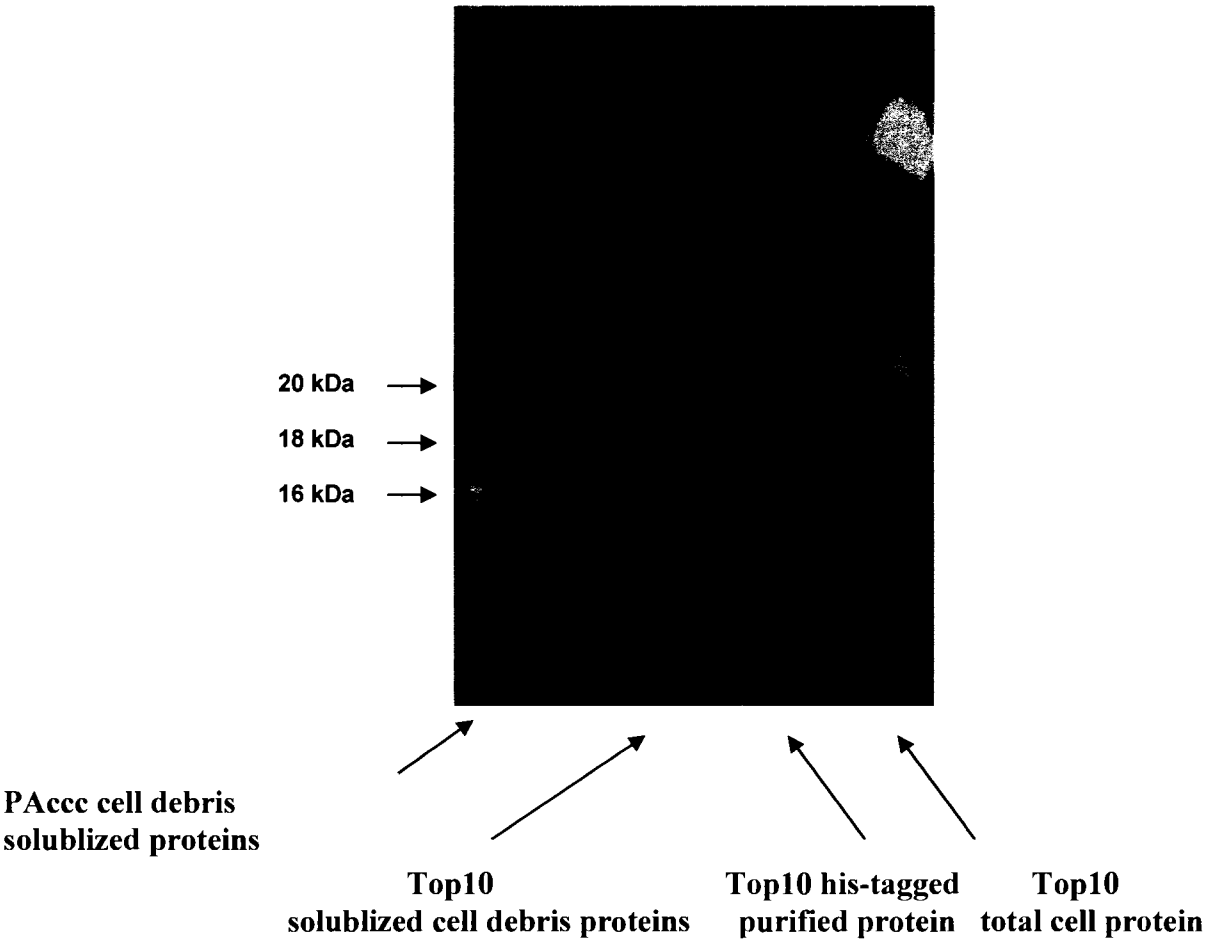
20 kDa
18 kDa
16 kDa
PAccc cell debris solublized proteins
Top10 solublized cell debris proteins
Top10 his-tagged purified protein
Top10 total cell protein

Figure 7. Replica samples of amplified PCR products of *un-24*^{PA} cDNA by un-24FWPA and un-24RVPA primers.

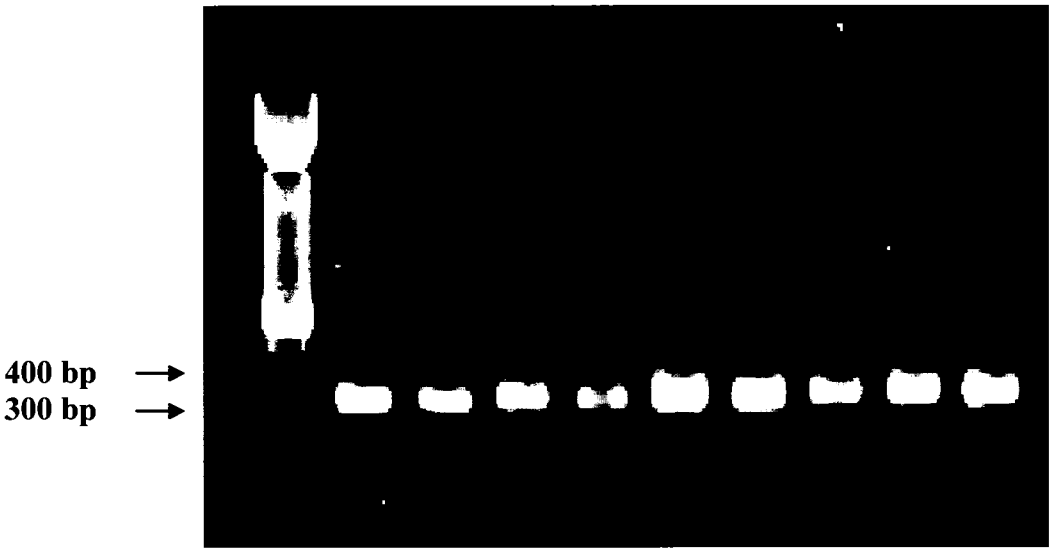
400 bp
300 bp

Figure 8. Nucleotide and amino acid sequences of PAccc clone. Start (atg) and stop (taa) sites are shown in green and introduced *Bam*HI and *Sal*I restriction enzyme sites in red and brown, respectively. Purple and blue represent 6-His tag and three conserved C-terminus cysteine residues of *un-24*^{PA} in PAccc clone, respectively. These cysteines, which are numbered 1-3, are responsible for protein complex formation that lead to incompatibility activity in *N. crassa*. Nucleotide numbers are shown in the left and right margins.

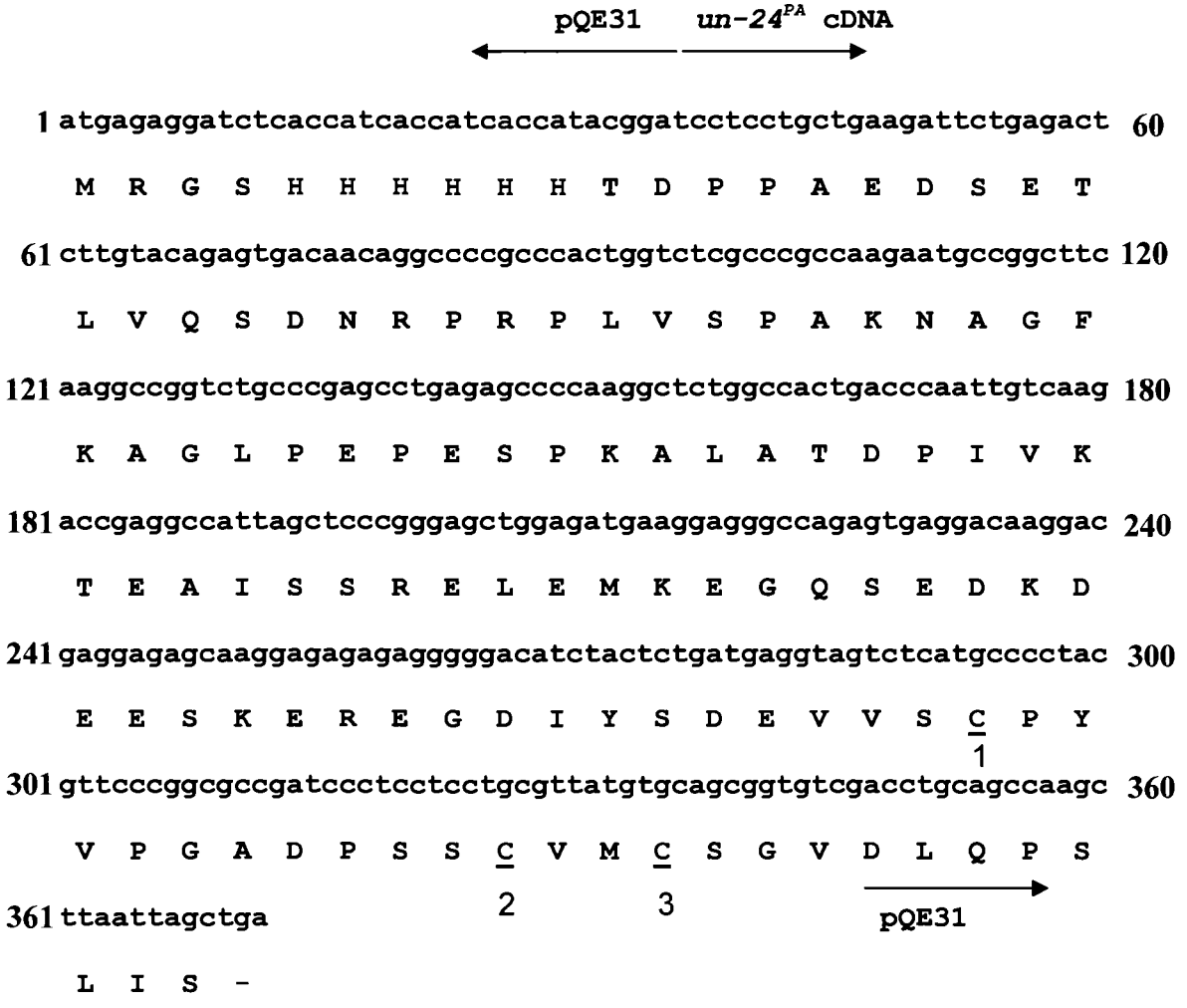
pQE31
un-24PA cDNA
1 atgagaggatctcaccatcaccatcaccatacggatcctcctgctgaagattctgagact 60
M R G S H H H H H H T D P P A E D S E T
61 cttgtacagagtgacaacaggccccgcccactggtctcgcccgccaagaatgccggcttc 120
L V Q S D N R P R P L V S P A K N A G F
121 aaggccggtctgcccgagcctgagagccccaaggctctggccactgacccaattgtcaag 180
K A G L P E P E S P K A L A T D P I V K
181 accgaggccattagctcccgggagctggagatgaaggagggccagagtgaggacaaggac 240
T E A I S S R E L E M K E G Q S E D K D
241 gaggagagcaaggagagagaggggacatctactctgatgaggtagtctcatgcccctac 300
E E S K E R E G D I Y S D E V V S C P Y
1
301 gttcccggcgccgatccctcctcctgcgttatgtgcagcggtgtcgacctgcagccaagc 360
V P G A D P S S C V M C S G V D L Q P S
2
3
pQE31
361 ttaattagctga
L I S -

Figure 9. Western blot of PAccc purified protein. Protein from induced cultures yielded two bands of 20 and 18 kDa when protein was treated under non-reducing conditions (lane 1), or with BME (lane 2), and revealed the third band at 16 kDa after reduction by BME and urea (lane 3), or BME and urea and DTT (lane 4). Reducing agents were added to the extraction buffers for protein purification under reducing conditions.

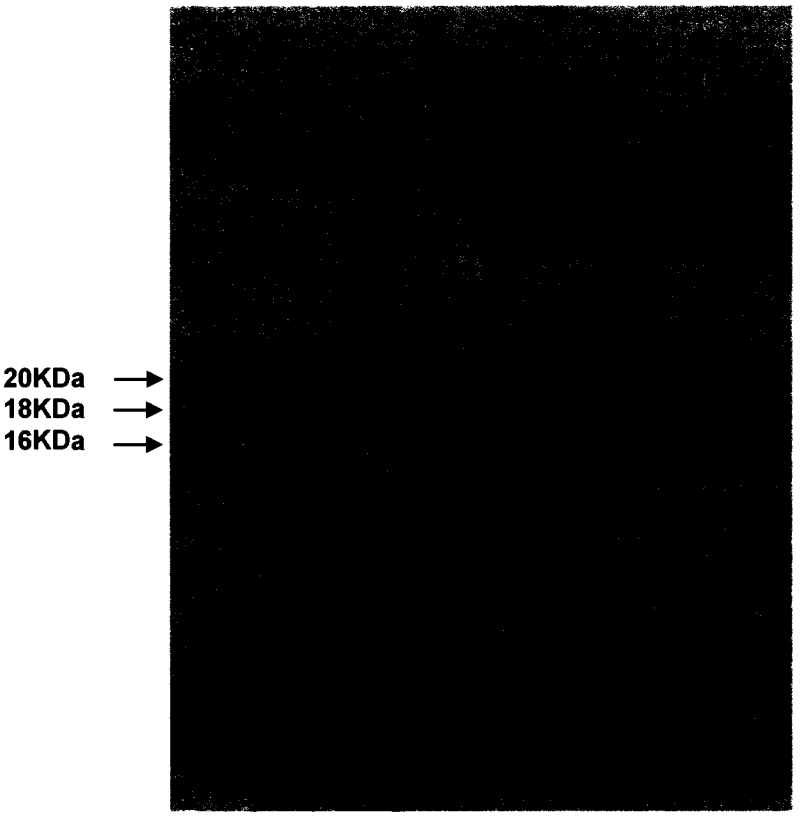
20KDa
18KDa
16KDa

Expressed protein* of *C-terminus cysteine mutants of* un-24^{PA} *have multiple forms, influenced by each of the cysteines

To obtain the cysteine mutant constructs, the rolling circle mutagenesis procedure was conducted to substitute one or more cysteine codons to glycine. PAccc clone was amplified by three different sets of primers to substitute first, second, or third cysteine to obtain single cysteine mutant constructs, PAgcc, PAcgc, and PAccg, respectively. Figure 10 shows amplification of 3,800 bp of PAccc plasmid by PAgcc primers. Other double and triple cysteine substitution mutants were also created by this method and expressed in Top10 cells. Figure 11 gives nucleotide and amino acid sequences of PAccc and seven cysteine mutant constructs.

All of the constructs shown in Figure 11 were verified by DNA sequencing, and then their respective proteins were expressed without induction and with induction under non-reducing and reducing conditions. Figures 12 – 14 show Western blots of extracted proteins of single, double and triple mutants, respectively. Figure 12 shows that the PAgcc protein is evident as only two bands of 20 and 18 kDa in all conditions. In contrast inducing the PAcgc protein produces an additional smaller band of 16 kDa under non-reducing conditions only. Protein of the PAccg clone revealed one band of 20 kDa in uninduced, two bands of 20 and 18 kDa in induced, and three bands of 20, 18, and 16 kDa in induced cultures extracted under reducing conditions. These three protein bands are identical in size to those produced by the wild type PAccc clone but show up under slightly different conditions. Again, each of the protein bands exceeds the expected 13.2 kDa size for this protein. Based on these electrophoretic mobility assays, this small peptide appears to take on multiple forms when expressed in *E. coli*, and these forms are

influenced by expression level and reducing conditions. Furthermore each of the three cysteines appears to influence the electrophoretic mobility of the peptide, suggesting that they have a role in determining the shape/mobility of the protein.

Figure 13 shows the electrophoretic pattern of each of the three possible double cysteine mutants, when non-induced and induced under non-reducing and reducing conditions. For each construct and treatment the 20 kDa band was evident, so that, as in the single cysteine mutants, this 20 kDa represents the most common form of the protein. In general, the 18 kDa band becomes more pronounced when extractions are done under reducing conditions. The 16 kDa band was evident only when the PAcgg construct was induced and protein was extracted under reducing conditions. Again, each of the three constructs has a unique electrophoretic pattern, indicating that the combination of presence and absence of cysteines has a subtle effect on the form of this small protein when expressed in *E. coli*. However, it is unknown what the oxidized forms represent; for example, given that each of the expressed proteins in Figure 13 has only a single cysteine, reducing conditions would not be breaking cysteine-associated disulfide bonds.

Figure 10. PCR-amplified 3,800 bp product of PAccc plasmid using two different concentrations of DNA template (0.2 and 0.3 µl of 137 ng/ µl in lane 1 and 2, respectively) and PAgcc primers to create the PAgcc construct.

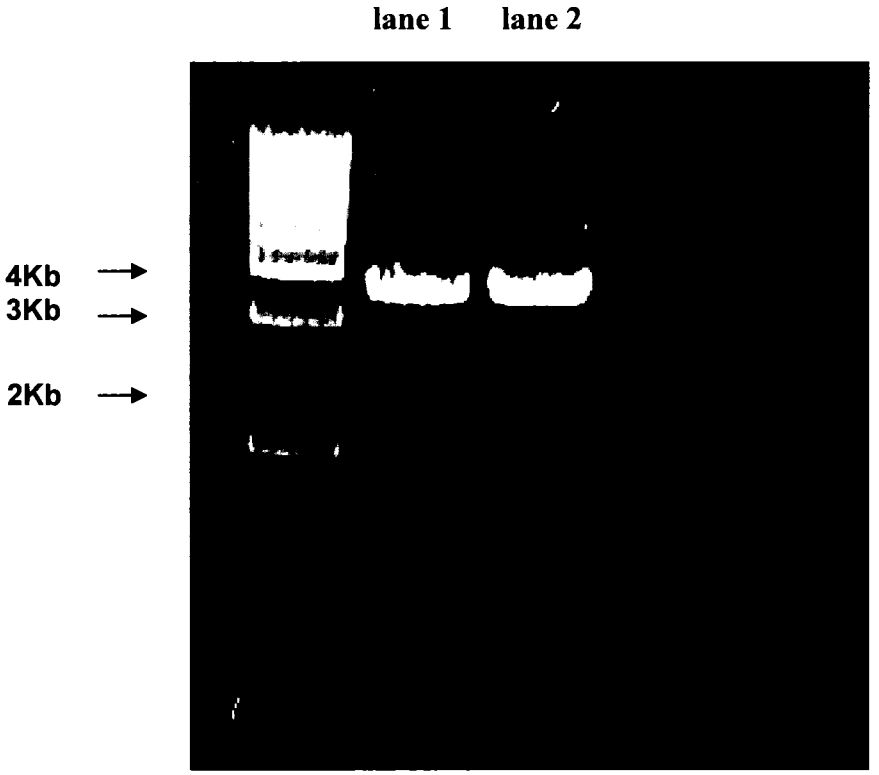
lane 1
lane 2
4Kb
3Kb
2Kb

Figure 11. Nucleotide and amino acid sequences of PAccc and derivative cysteine mutant constructs. In these constructs, 1 – 3 cysteines (in blue) were changed to glycine as indicated by substitutions shown in red. Nucleotide numbers are provided with reference to the complete expressed coding region, as in Figure 8.

PAccc 285 gtctcatgcccctacgttcccggcgccgatccctcctcctgcgttatgtgcagc 339

V S C P Y V P G A D P S S C V M C S

1 2 3

PAgcc 285 gtctcaggcccctacgttcccggcgccgatccctcctcctgcgttatgtgcagc 339

V S G P Y V P G A D P S S C V M C S

2 3

PAcgc 285 gtctcatgcccctacgttcccggcgccgatccctcctccggcgttatgtgcagc 339

V S C P Y V P G A D P S S G V M C S

1 3

PAccg 285 gtctcatgcccctacgttcccggcgccgatccctcctcctgcgttatgggcagc 339

V S C P Y V P G A D P S S C V M G S

1 2

PAggc 285 gtctcaggcccctacgttcccggcgccgatccctcctccggcgttatgtgcagc 339

V S G P Y V P G A D P S S G V M C S

3

PAgcg 285 gtctcaggcccctacgttcccggcgccgatccctcctcctgcgttatgggcagc 339

V S G P Y V P G A D P S S C V M G S

2

PAcgg 285 gtctcatgcccctacgttcccggcgccgatccctcctccggcgttatgggcagc 339

V S C P Y V P G A D P S S G V M G S

1

PAggg 285 gtctcaggcccctacgttcccggcgccgatccctcctccggcgttatgggcagc 339

V S G P Y V P G A D P S S G V M G S

Figure 12. Western blot of proteins extracted from single cysteine mutant constructs PAgcc, PAcgc and PAccg reveal different banding patterns. The lanes represent uninduced (red labels) and induced samples isolated under non-reducing conditions (green labels) and reducing conditions (BME and urea, blue labels).

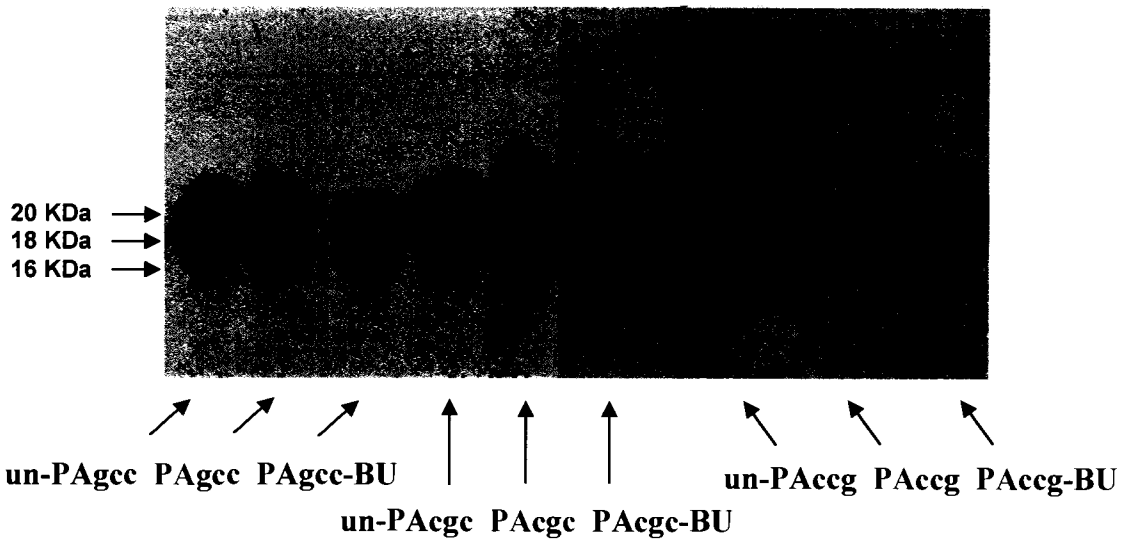
20 KDa
18 KDa
16 KDa
un-PAgcc
PAgcc
PAgcc-BU
un-PAcgc
PAcgc
PAcgc-BU
un-PAccg
PAccg
PAccg-BU

Figure 13. Western blot of purified proteins from double mutant constructs of PAcgg, PAggc and PAgcg. The lanes represent uninduced (red labels) and induced samples isolated under non-reducing conditions (green labels) and reducing conditions (BME and urea, blue labels).

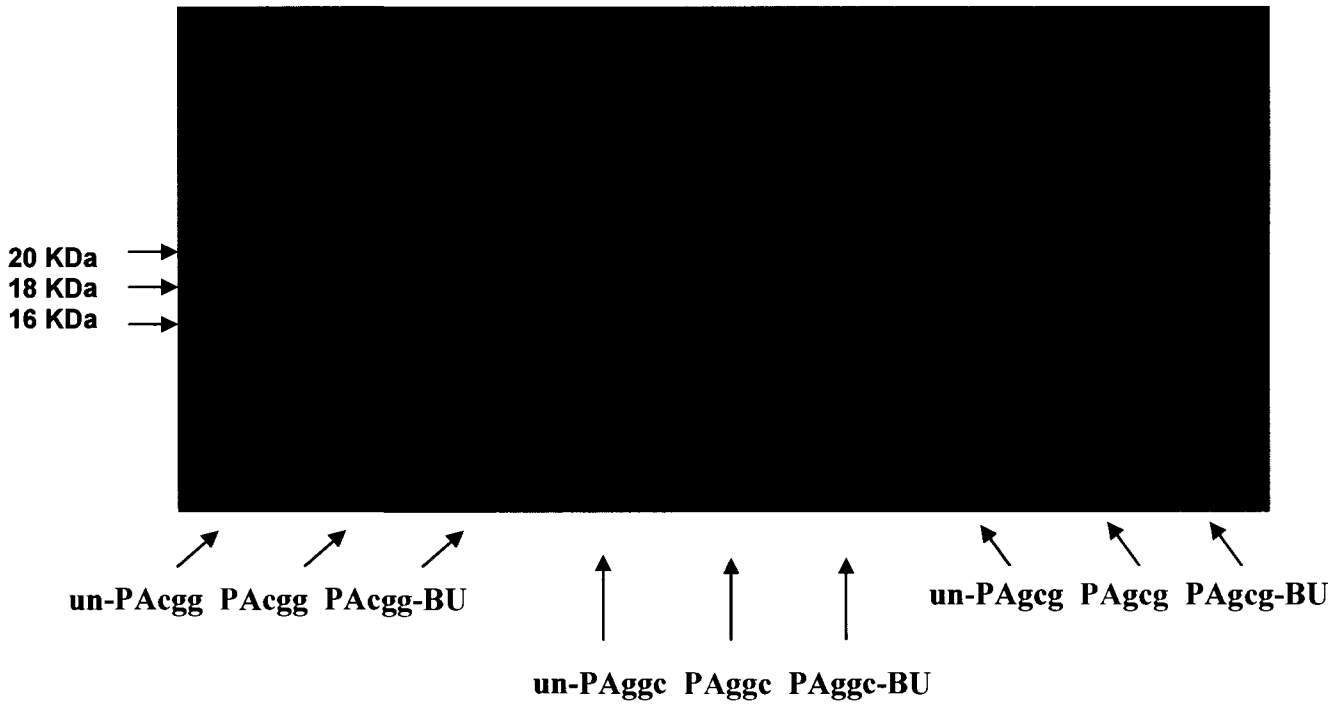
20 KDa
18 KDa
16 KDa
un-PAcgg
PAcgg
PAcgg-BU
un-PAggc
PAggc
PAggc-BU
un-PAgcg
PAgcg
PAgcg-BU

Effect of deletion of the last twelve amino acids of C-terminus protein

Figure 14 shows the electrophoretic patterns of two additional mutant forms of the C-terminus of UN-24. At the left of this figure is shown electrophoretic patterns of the deletion mutant, PAgc, which was expressed in the vector pQE30UA and has the first cysteine substituted to a glycine and the last 12 amino acids including the third (most C-terminal) cysteine deleted. This expressed protein resolves as a single band in each of the treatments, implicating this most C-terminal region that is deleted in the multiple forms of the protein. Compared to the other proteins dealt with so far that were expressed in the pQE31 vector, the pQE30UA incorporates an additional 10 amino acids into the N-terminus region of the expressed protein (Figure 15). Nevertheless, the observed size from this Western blot of the PAgc purified protein was 18 kDa, again significantly larger than the expected size of 12.8 kDa for this protein. Therefore, elements in the remaining portion of this small protein must be responsible for its low electrophoretic mobility. Aside from the size difference, the PAgc deletion form looks very similar to the PAgcg protein (Figure 13), which also mainly presented a single protein band. Based on these observations, it is plausible that cysteine 2 crosslinks to one of cysteines 1 or 3 to yield the additional protein bands seen on Western blots. However, this idea is not supported by the protein profile of the final construct, PAggg (Figure 14). All three cysteines were substituted for glycine in the PAggg construct and it produced the 20 kDa protein form only in non-induced cultures and all three (20, 18 and 16 kDa) bands were evident in induced cultures, whether or not they were extracted under reducing or non-reducing conditions. Taken together these electrophoretic patterns implicate each of the three cysteines and the very C-terminus region, deleted in the PAgc construct, in the

observed complex of form changes evident for this small protein. Finally, a comparison of band sizes and patterns of PAccc and all the derived mutant forms is presented in Figure 16.

Figure 14. Western blot of proteins from PAgc-deletion and PAggg clones. The lanes represent uninduced (red labels) and induced samples isolated under non-reducing conditions (green labels) and reducing conditions (BME and urea, blue labels).

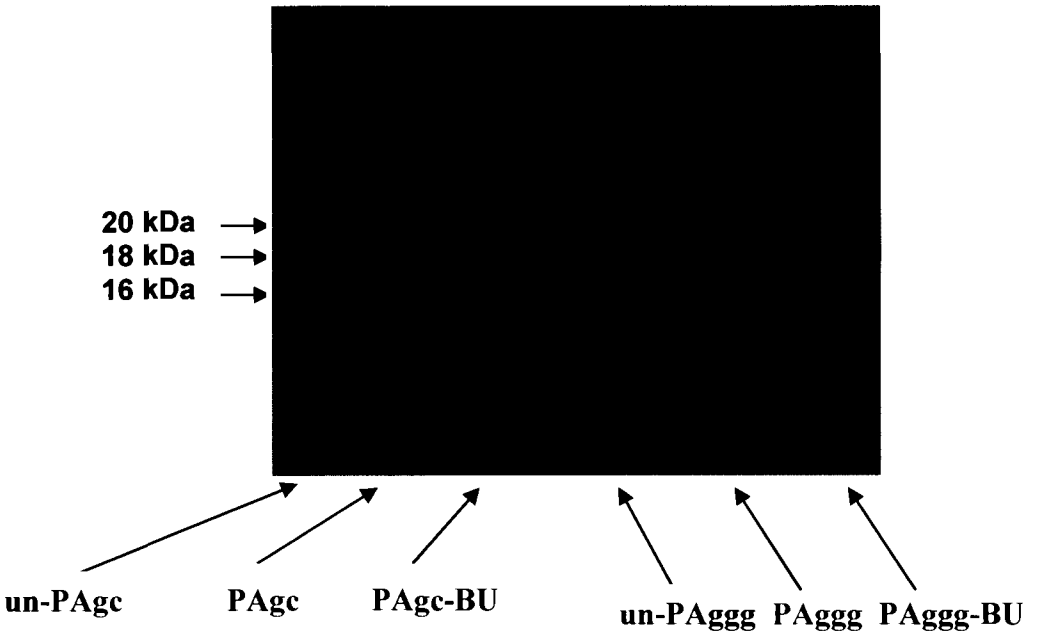
20 kDa
18 kDa
16 kDa
un-PAgc
PAgc
PAgc-BU
un-PAggg
PAggg
PAggg-BU

Figure 15. Sequence of nucleotides and amino acids of PAgc-deletion construct. Green nucleotides represent start and stop codons and 6-His tag is shown in purple. Additional 10 amino acids encoded by pQE30UA vector, which are not present in pQE31-expressed proteins, is shown in yellow-brown colour. Substituted cysteine to glycine positions is shown in red and cysteine 2 is in blue.


1 atgagaggatcgcatcaccatcaccatcacggatcccacgtgatatcctcaatcgcttct 60
M R G S H H H H H H G S H V I S S I A S
pQE31
un-24^PA cDNA
61 acggatcctcctgctgaagattctgagactcttgtacagagtgacaacaggccccgccca 120
T D P P A E D S E T L V Q S D N R P R P
121 ctggtctcgcccgccaagaatgccggcttcaaggccgatctgcccgagcctgagagcccc 180
L V S P A K N A G F K A D L P E P E S P
181 aaggctctggccactgacccaattgtcaagaccgaggccattagctcccgggagctggag 240
K A L A T D P I V K T E A I S S R E L E
241 atgaaggagggccagagtgaggacaaggacgaggagagcaaggagagagaggggacatc 300
M K E G Q S E D K D E E S K E R E G D I
301 tactctgatgaggtagtctcaggcccctacgttcccggcgccgatccctcctcctgctga 360
Y S D E V V S G P Y V P G A D P S S C -
1
2

Figure 16. Summary comparison of protein band sizes and patterns of PAccc and derived mutant constructs. Top, middle, and bottom arrows represent 20, 18, and 16 kDa molecular weights. Also, black, gray, and white arrows represent strong, weak, and no band, respectively, based on at least three Westerns for each construct.

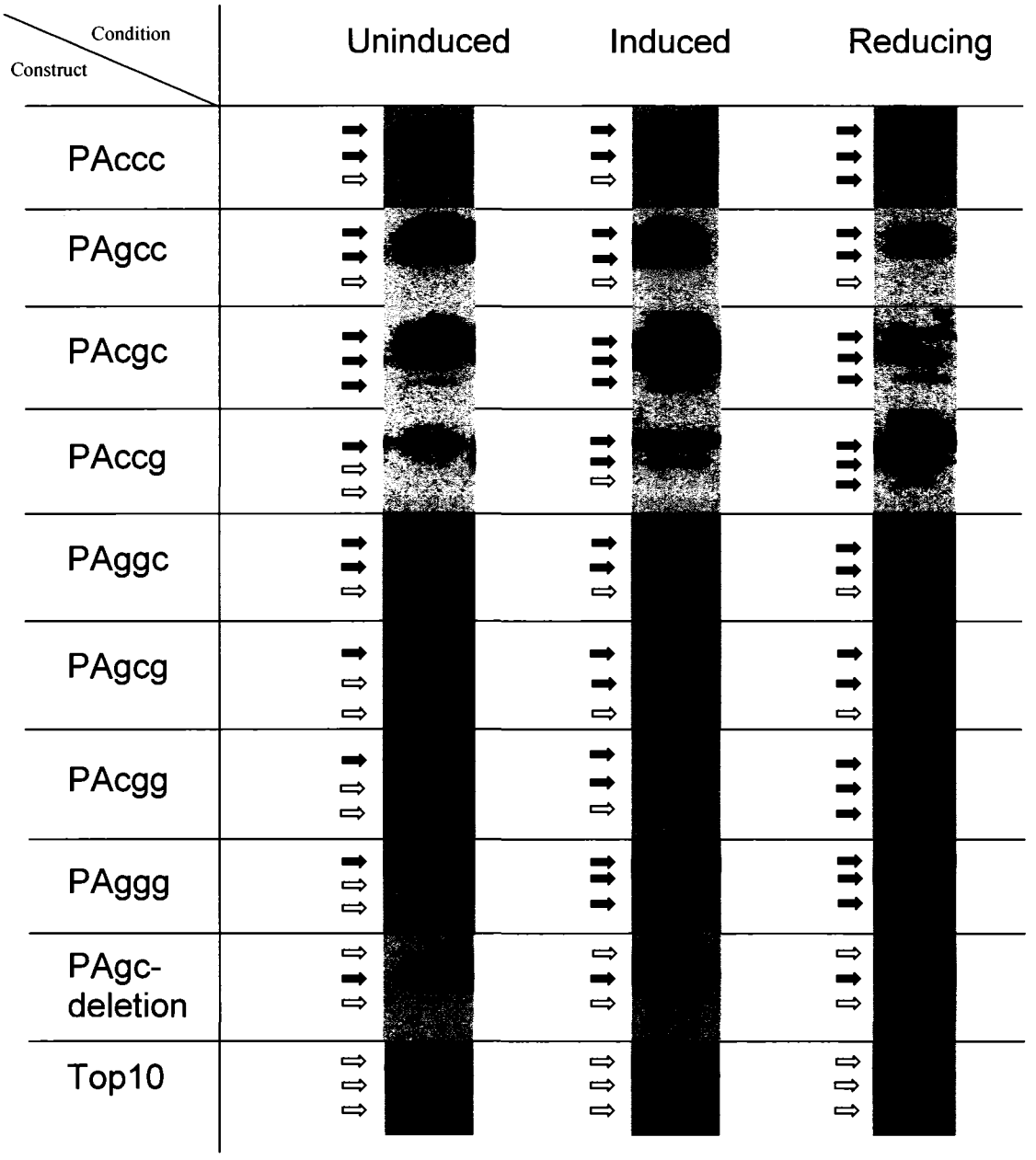
Condition
Construct
Uninduced
Induced
Reducing
PAccc
PAgcc
PAcgc
PAccg
PAggc
PAgcg
PAcgg
PAggg
PAgc-deletion
Top10

DISCUSSION

The purpose of this study was to express the C-terminal region from the *N. crassa* large subunit of ribonucleotide reductase, and to carry out an initial characterization of physical properties of this protein region. First, I cloned 306 bp of the C-terminus domain of *un-24*^{PA}, and expressed it in *E. coli*. This produced two bands of 20 and 18 kDa, both larger than the expected size of 13.2 kDa. The large size of these protein bands was hypothesized to be due to disulfide bond formation between two of the three cysteine residues in this protein. C-terminal cysteines are involved in redox reactions of RNR by reducing of active site disulfide (Ge *et al.*, 2003) and this region was found to be sufficient to cause cross linking to the OR form of UN-24 in both *N. crassa* (Wellman *et al.*, unpublished) and to the resident homolog, RNR1, in yeast (R. Smith, unpublished). Therefore, the expressed PAccc protein was purified under reducing conditions. While the large 20 and 18 kDa protein bands were still evident under reducing conditions, the presence of a novel 16 kDa band suggested the occurrence of disulfide bridge cleavage within the protein. To further test whether or not cysteine cross linking was involved in the electrophoretic resolution of multiple large bands, I created seven cysteine constructs by substituting cysteine to glycine codons. Expressed proteins of the cysteine substituted constructs showed changes in the protein banding patterns. These changes all appeared to be based on variations of whether or not each of the three major protein bands appeared at 20, 18 and 16 kDa. No other significant size shifts were evident, aside from that of PAgc, which had both an insertion (in the N-terminus region) and a deletion (in the C-terminus region)

Although the electrophoretic banding patterns are complex, some common characteristics may be observed. First, substitution in the first, or first and second cysteines, in PAgcc and PAggc mutants, had very similar banding patterns; both had bands in 20 and 18 kDa size range under all treatment conditions. In addition, PAccg and PAcgg, constructs which were both substituted in the third cysteine, had the same band patterns of: one 20 kDa in un-induced, two 20 and 18 kDa in induced, and 20, 18, and 16 kDa when induced and extracted under reducing conditions. A clear modification of the two or three protein banding patterns was evident in the PAgc construct. This protein has the C-terminal region deleted and consistently produced a single protein band under all extraction conditions. This construct suggests that a residue(s) other than the third cysteine located within the last 12 amino acids from the C-terminus is somehow responsible for the multiple protein bands evident with all other constructs.

The PAgc C-terminus deletion construct still ran out in SDS-PAGE gels at a larger size than theoretically expected. This slow mobility characteristic is common to all of the constructs examined in this thesis. This mobility shift could be due to the sequence composition of this small expressed protein. One feature that may be relevant to these low migration rates is the relatively large number of proline residues in the expressed protein. From Figure 8 it can be seen that there are 13 proline residues distributed along the 123 amino acids of the expressed PAccc protein. Prolines are known to cause "kinks" in the protein chain and are not compatible with some secondary structures such as α-helixes and may regulate the mechanical stretching of the protein (Arteca and Li, 2004). Such kinks may be essential for proper folding of the C-terminus of UN-24, to enable its proper insertion into the catalytic site and permit disulfide exchange and restoration of

catalytic activity of the enzyme. An abundance of such kinks may reduce the rate of movement by the protein through the SDS-PAGE gel.

Alternatively, *E. coli* cells may introduce some post-translational modification effects on the proteins that were expressed in this study, such as phosphorylation, which may effect protein mobility in SDS-PAGE. According to Macek *et al.* (2008), protein phosphorylation of serine, threonine, and tyrosine is a common regulatory posttranslational modification in *E. coli* cells. Addition of a negatively charged phosphate group to the protein would make it run slower in SDS-PAGE. However, addition of phosphate groups to the expressed protein does not, in itself, explain the different patterns observed with some cysteine mutant constructs when reducing conditions were used during the extraction process.

In addition to cysteine crosslinking, which appears to have a minor effect in producing the multiple electrophoretic bands observed, there is the possibility that other non-reducible cross links may be formed within this protein. As discussed in the introduction to this thesis, the current model of how the C-terminus causes heterokaryon incompatibility involves a non-reducible crosslinking to residues in the catalytic site. Non-reducible amino acid linkages such as cysteine-tyrosine have been documented (Firbank *et al.*, 2001) and these could affect the electrophoretic mobility of the proteins expressed in this study. Myristoylation, is another irreversible post-translational modification that occurs by the covalent addition of a myristoyl group on amino acids (mostly glycine). However, myristoylated proteins migrate faster than the non-myristoylated forms (Sikorski *et al.*, 1997). These possible forms of crosslinking could be

tested by comparing profiles of the expressed protein developed in this thesis using proteolytic digests followed by mass spectroscopy (Bothner *et al.*, 1998).

I verified that Top10 cells that did not contain a 6-His-expressing vector did not produce any proteins that cross-reacted with the anti-6-His antibody. Also all constructs were expressed in both un-induced and induced conditions. It is noted that the un-induced condition still produced a large quantity of the expressed protein. Nevertheless, it appeared that addition of IPTG did up-regulate protein expression and this was generally evident from both larger amounts of protein in the induced condition and, in some cases, different electrophoretic profiles. This later observation suggests that the abundance of protein expressed by *E. coli* influences the crosslinking or other modifications that were responsible for the electrophoretic patterns observed. Given that the Top10 cells used in my expression experiments do not apparently tightly regulate transcription. Using the *lacI* regulatory system, other *E. coli* strains that do so may be expected to produce altered electrophoretic patterns from those seen in my experiments. This would be interesting to pursue with *E. coli* strains that harbour the *lacIq* mutation, such as XL1 Blue, JM109 and TG1 that all produce enough *lac* repressor to efficiently block transcription in uninduced cultures. It is possible that using these other *E. coli* strains may cause a change in the form of the expressed proteins.

While this system appears to be complex, I observed that the electrophoretic results presented are very reproducible. Only the third band, in the 16 kDa range was visible in some, but weak or not visible in other of the replicate experiments. Overall, then, it appears that the small protein domain at the C-terminus of the large subunit of ribonucleotide reductase is predictably modified during expression in *E. coli*.

FUTURE STUDIES

Generating polyclonal antibody to the C-terminus region of *un-24*^{PA} that was expressed in this study is now possible and will be useful for several experiments that aim to understand the nonself recognition system in *N. crassa*. Future cloning of the *un-24*^{OR} full-length cDNA in pQE31 vector would give the opportunity to conduct *in vitro* protein-protein interaction experiments between the *un-24*^{PA} cysteine mutant proteins and the full-length *un-24*^{OR} protein. While difficult, mutations of other residues, such as the multiple prolines discussed above, could possibly alter the mobility patterns of this protein.

REFERENCES

Åberg A, Hahne S, Karlsson M, Larsson Å, Ormö M, Åhgren A, and Sjöberg B-M (1989) Evidence for two different classes of redox-active cysteines in ribonucleotide reductase of *Escherichia coli.* J Biol Chem. 264(21):12249-52

Arteca GA, and Li Z (2004) Effect of proline kinks on the mechanical unfolding of a-helices. Chem Phys Lett. 399 (4-6) 496–502

Balguerie A, Dos Reis S, Coulary-Salin B, Chaignepain S, Sabourin M, Schmitter J-M, and Saupe SJ (2004) The sequences appended to the amyloid core region of the HET-s prion protein determine higher-order aggregate organization *in vivo*. J Cell Sci. 117(Pt 12):2599-610

Balguerie A, Dos Reis S, Ritter C, Chaignepain S, Coulary-Salin B, Forge V, Bathany K, Lascu I, Schmitter J-M, Riek R, and Saupe SJ (2003) Domain organization and structure-function relationship of the HET-s prion protein of *Podospora anserina.* EMBO J. 22(9):2071-81

Bleifuss G, Kolberg M, Pötsch S, Hofbauer W, Bittl R, Lubitz W, Gräslund A, Lassmann G, and Lendzian F (2001) Tryptophan and tyrosine radicals in ribonucleotide reductase: acomparative high-field EPR study at 94 GHz. Biochem (40) 15362-15368

Biella S, Smith ML, Aist JR, Cortesi P, and Milgroom MG (2002) Programmed cell death correlates with virus transmission in a filamentous fungus. Proc Biol Sci. 269(1506):2269-76

Booker S, Licht S, Broderick J, and Stubbe J (1994) Coenzyme B12-dependent ribonucletoide reductase: evidence for the participation of five cysteine residues in ribonucleotide reduction. Biochem. 33(42):12676-85

Bothner B, Dong XF, Bibbs L, Johnson JE, and Siuzdak G (1998) Evidence of Viral Capsid Dynamics Using LimitedProteolysis and Mass Spectrometry. J Biol Chem. 273(2): 673–676

Cortesi P, McCulloch CE, Song H, Lin H, and Milgroom MG (2001) Genetic control of horizontal virus transmission in the chestnut blight fungus, *Cryphonectria parasitica.* Genet. 159(1):107-18

Coustou-Linares V, Maddelein M, Bégueret J , and Saupe SJ (2001) *In vivo* aggregation of the HET-s prion protein of the fungus *Podospora anserina.* Mol Microbiol. 42(5):1325-35

Debets AJM, and Griffiths AJF (1998) Polymorphism of *het* genes prevents resource plundering in *Neurospora crassa.* Mycol. Res. 102:1343-49

Deleu C, Clavé C, Bégueret J (1993) A single amino acid difference is sufficient to elicit vegetative incompatibility in the fungus *Podospora anserina*. Genet. 135(1):45-5

Ekland H, Uhlin U, Färnegårdh M, Logan DT, and Nordlund P (2001) Structure and function of the radical enzyme ribonucletide reductase. Biophys Mol Biol 77(3): 177-268

Elledge SJ, Zhou Z, Allen JB, Navas TA (1993) DNA damage and cell cycle regulation of ribonucleotide reductase. Bioessays. 15(5):333-9

Eriksson M, Uhlin U, Ramaswamy S, Ekberg M, Regnstorm K, Sjöberg B-M, and Eklund H (1997) Binding of allosteric effectors to ribonucleotide reductase protein R1: reduction of active site cysteines promotes substrate binding. Structure 5(8)1077-92

Espagne E, Balhadère P, Penin ML, Barreau C, Turcq B (2002) HET-E and HET-D belong to a new subfamily of WD40 proteins involved in vegetative incompatibility specificity in the fungus *Podospora anserina*. Genet. 161(1):71-81

Firbank SJ, Rogers MS, Wilmot CM, Dooley DM, Halcrow MA, Knowles PF, McPherson MJ, and Phillips SE (2001) Crystal structure of the precursor of galactose oxidase: an unusual self-processing enzyme. Proc Natl Acad Sci U S A. 98(23): 12932–12937.

Fontecave M, (1998) Ribonucleotide reductase and radical reactions. Cell Mol Life Sci. (54) 684-695

Ge J, Yu G, Ator MA, and Stubbe J (2003) Pre-steady state and steady- state kinetic analysis of *E. coli* classI ribonucleotide reductase. Biochem. (42) 10071- 10083

Gibbs C (2004) Nonself recognition in *Neurospora crassa* and *Cryphonectria parasitica.* MSc. Thesis. Carleton University, Ottawa, Ontario

Glass NL, Jacobson DJ, Shiu PK (2000) The genetics of hyphal fusion and vegetative incompatibility in filamentous Ascomycete fungi. Annu Rev Genet. 34:165-186

Glass NL, and Kaneko I (2003) Fatal attraction: Nonself recognition and heterokaryon incompatibility in filamentous fungi. Eukaryot Cell. 2(1):1-8

Glass N L, and Kuldau GA (1992) Mating type and vegetative incompatibility in filamentous ascomycetes. Annu Rev Phytopathol. 30:201-24

Haidari L (2002) Incompatibility activity and expression of ribonucleotide redoctase in Neurospora crassa. MSc. Thesis. Carleton University, Ottawa, Ontario

Hamann A, Brust D, and Osiewacz HD (2008) Apoptosis pathways in fungal growth, development and ageing. Trends Microbiol. 16(6):276-83

Jacobson MD (1997) Programmed cell death: a missing link is found. Trends Cell Biol. 1997(12):467-9

Jacobson DJ, Beurkens K, and Klomparens KL (1998) Microscopic and Ultrastructural Examination of Vegetative Incompatibility in Partial Diploids Heterozygous at het Loci in *Neurospora crassa*. Fungal Genet Biol. 23(1):45-56

Kaneko I, Dementhon K, Xiang Q, and Glass NL (2006) Nonallelic interaction between *het-c* and a polymorphic locus, *pin-c*, are essential for nonself recognition and programmed cell death in *Neurospora crassa*. Genet. 172(3): 1545-1555

Kasrayan A, Birgander PL, Pappalardo L, Regnström K, Westman M, Slaby A, Gordon E, and Sjöberg B-M (2004) Enhancement by effectors and substrate nucleotides of R1-R2 interactions in *Escherichia coli* class Ia ribonucleotide reductase. J Biol Chem. 279(30): 31050-7

Kolberg M, Strand KR, and Andersson KK (2004) Structure, function, and mechanism of ribonucleotide reductase. Biochim Biophys Acta. 1699(1-2):1-34

Lee YD, and Elledge SJ (2006) Control of ribonucletide reductase localization through an anchoring mechanism involving Wtm1. Genes Dev. 20(3):334-44

Leslie JF, Yamashiro CT (1997) Effects of the tol mutation on allelic interactions at het loci in Neurospora crassa. Genome. 40(6):834-40

Lin A-N I, Ashley GW, and stubbe J (1987) Location of redox active thiols of ribonucleotide reductase: sequence similarity between the *Escherichia coli* and *Lactobacillus Leichmannii* enzymes. Biochem. 26(22):6905-9

Loubradou G, Bégueret J, Turcq B (1999) *MOD-D, a* $G\alpha$ subunit of the fungus *Podospora anserina,* is involved in both regulation of development and vegetative incompatibility, Geneti. 152(2):519-28

Mao SS, Holler TP, YU Gx, Bollinger JM, Jr, Booker S, Johnston MI, and Stubbe J (1992) A model for role of multiple cysteine residues involved in ribonucleotide reductase: amazing and still confusing. Biochem. 31(40): 9733-43

Marek S M, Wu J, Glass NL, Gilchrist DG, and Bostock RM (2003) Nuclear DNA degradation during heterokaryon incompatibility in *Neurospora crassa.* Fungal Genet Biol. 40(2):126-37

Macek B, Gnad F, Soufi B, Kumar C, Olsen JV, Mijakovic I, and Mann M (2008) Phosphoproteome Analysis of *E. coli* Reveals Evolutionary Conservation of Bacterial Ser/Thr/Tyr Phosphorylation. Mol and Cell Prot. 7:299-307

Micali CO, and Smith ML (2006) A nonself recognition gene complex in *Neurospora crassa*. Genet. 173(4):1991-2004. Epub 2006 Jun 4

Mir-Rashed N, Jacobson DJ, Dehghany MR, Micali OC, Smith ML (2000) Molecular and functional analyses of incompatibility genes at het-6 in a population of Neurospora crassa. Fungal Genet Biol. 30(3):197-205

Mulliez E, Fontecave M, Jaques G, and Reichard P (1993) An iron-sulfur centre and a free radical in the active anaerobic ribonucleotide reductase of *Escherichia coli*. J Biol Chem. 268(4):2296-9

Nordlund P, and Eklund H (1993) Structure and function of *Escherichia coli* ribonucletide reductase R2. J Mol Biol. 232(1):123-64

Pál K (2005) Vegetative incompatibility in *Aspergillus niger*. Acta Biologica Szegediensis. 49(3-4):57

Perkins DD (1988) Main features of vegetative incompatibility in *Neurospora.* Fungal Genet News l (34) 44-46

Persson AL, Sahlin M, and Sjoberg B-M (1998) Cysteinyl and substrate radical formation in active site mutant E441Q of *Escherichia coli* class I ribonucleotide reductase. J Biol Chem. 273(47):31016-2

Peter R, (2002) Ribonucleotide reductase: The evalution of allosteric regulation. Arch Biochem Biophys 397(2): 149-155

Pinan-Lucarré B, Paoletti M, Dementhon K, Coulary-Salin B, Clavé C (2003) Autophagy is induced during cell death by incompatibility and is essential for differentiation in the filamentous fungus *Podospora anserina*. Mol Microbiol. 47(2):321-33

Romano N, and Macino G (1992) Quelling: transient inactivation of gene expression in *Neurospora crassa* by transformation with homologous sequences. Mol Microbiol. 6(22):3343-53

Saupe SJ (2000) Molecular Genetics of Heterokaryon Incompatibility in Filamentous Ascomycetes. Microbiol Mol Biol Rev. 64(3):489-502

Saupe S J, Clavé C, Bégueret J (2000) Vegetative incompatibility in filamentous fungi: *Podospora* and *Neurospora* provide some clues. Curr Opin Microbiol. 3(6):608-12

Saupe SJ, and Glass NL (1997) Allelic specificity at the het-c heterokaryon incompatibility locus of *Neurospora crassa* is determined by a highly variable domain. Genetics. 146(4):1299-309

Saupe SJ, Kuldau GA, Smith ML, and Glass NL (1996) The product of the het-C heterokaryon incompatibility gene of *Neurospora crassa* has characteristics of a glycine-rich cell wall protein. Genet. 143(4):1589-600

Shiu PK, and Glass NL (1999) Molecular characterization of tol, a mediator of mating-type-associated vegetative incompatibility in *Neurospora crassa.* Genet. 151(2):545-55

Sikorski JA, Devadas B, Zupec ME, Freeman SK, Brown DL, Lu HF, Nagarajan S, Mehta PP, Wade AC, Kishore NS, Bryant ML, Getman DP, McWherter CA, and Gordon JI (1997) Selective peptidic and peptidomimetic inhibitors of Candida albicans myristoylCoA: protein N-myristoyltransferase: a new approach to antifungal therapy. Biopolymers. 43(1):43-71

Smith ML, Gibbs CC, and Milgroom MG (2006) Heterokaryon incompatibility function of barrage-associated vegetative incompatibility genes (vic) in Cryphonectria parasitica. Mycologia. 98(1):43-50

Smith ML, Hubbard SP, Jacobson DJ, Micali OC, and Glass NL (2000) An osmatic-remedial, temperature-sensitive mutation in the allosteric activity site of ribonucleotide reductase in *Neurospora crassa.* Mol Gen Genet. 262(6):1022-35

Smith ML, Micali OC, Hubbard SP, Mir-Rashed N, Jacobson DJ, and Glass NL (2000) Vegetative incompatibility in the het-6 region of *Neurospora crassa* is mediated by two closely linked gene. Genet. 155(3):1095-104

Smith ML, Yang CJ, Metzenberg RL, and Glass NL (1996) Escape from het-6 incompatibility in Neurospora crassa partial diploids involves preferential deletion within the ectopic segment. Genet. 144(2):523-31

Staben C and Yanofsky C (1990) Neurospora crassa a mating-type region. Proc Natl Acad Sci U S A. 87(13):4917-21

Uhlin U, and Eklund H (1994) Structure of ribonucleotide reductase protein R1. Nature 370: 533-39

Wu J, and Glass NL (2000) Identification of specificity and generation of alleles with novel specificity at the het-c heterokaryon incompatibility locus of *Neurospora crassa.* Mol Cell Biol. 21(4):1045-57

Xiang Q, and Glass NL (2002) Identification of vib-1, a locus involved in vegetative incompatibility mediated by het-c in *Neurospora crassa.* Genetics. 162(1):89-101

Xiang Q, and Glass NL (2004) Chromosome rearrangements in isolates that escape from *het-c* heterokaryon incompatibility in *Neurospora crassa.* Curr Genet 44(6): 329-338

Xiang Q, and Glass NL (2004) The control of mating type heterokaryon incompatibility by *vib-1*, a locus involved in het-c hetrokaryon incompatibility in *Neurospora crassa*. Fungal Genet Biol. 41(12):1063-76

Xu H, Faber C, Uchiki T, Racca J, and Daelwis C (2006) Structures of eukaryotic ribonucleotide reductase I define gemcitabine diphosphate binding and subunit assembly. Proc Natl Acad Sci U S A. 103(11):4028-33